Supplementary Information

for

Genetically controlled membrane synthesis in liposomes

by

Duco Blanken et al.

SUPPLEMENTARY METHODS

Cloning of *yfp-spinach* constructs for gene regulation experiments

The *eYFP-LL-spinach* construct was synthesised by Eurogentech (Belgium) and supplied in a pUC57 vector backbone [1]. A lac operator site was introduced via PCR using primers 715 and 716, and *E. coli* TOP10 cells were transformed with the obtained PCR fragment. The T7 promoter in pUC57-T7p-LacO-meYFP-LL-spinach-T7t was substituted with the SP6 promoter using primers 719 and 720 (**Supplementary Table 2**) and the generated pUC57-SP6p-LacO-meYFP-LL-spinach-T7t was used for transformation of TOP10 *E. coli* cells. The identity of the plasmids was confirmed with restriction digestion and Sanger sequencing.

Promoter orthogonality assay

Reaction mixtures consisted of a custom made PURE*frex*2.0 devoid of the T7 RNA polymerase (Cosmo Bio, USA). Either 8.1 μg μL^{-1} of T7 RNA polymerase or 4 U μL^{-1} SP6 RNA polymerase (Promega, USA) were added. The T7 RNA polymerase was overexpressed from a gene cloned into pBAD33 and isolated following the protocol of He et al. [2]. 7 nM of plasmid DNA (either pUC57-T7p-LacO-meYFP-LL-spinach-T7t or pUC57-SP6p-LacO-meYFP-LL-spinach-T7t was added last to trigger transcription-translation. Reaction samples of 10 μL were loaded into Greiner 384-well glass bottom plates sealed with a transparent foil and measured in a Tecan Infinite 200 Pro platereader (Tecan, Switzerland) with the temperature set to 37 °C. The excitation wavelength was 506 nm (9 nm bandwidth), the emission wavelength was 540 nm (20 nm bandwidth), and each measurement consisted of 25 flashes of 20 μs. Fluorescence of YFP was measured for 12 h with an interval time of 5 min. For each kinetic measurement, the data point of the highest fluorescence intensity was selected for further analysis.

SUPPLEMENTARY NOTES

Supplementary Note 1: Rational for gene orientation in pGEMM7

In a previous version of the plasmid (pGEMM6) both *pgsA* and *pgpA* genes were under control of an SP6 promoter but orientated in the same direction as the other genes on the plasmid (**Supplementary Fig. 4a**). We investigated whether PG production was conditional to the presence of SP6 RNAP. Plasmid pGEMM6 was expressed in PURE system containing LUVs and lipid synthesis was assessed by mass spectrometry. DOPG was produced also in the absence of SP6 RNAP (**Supplementary Fig. 4b**), showing the lack of transcriptional orthogonality. We suspected that read-through transcription might be the cause of unintended production of *pgsA* and *pgpA* transcripts, eventually leading to PG synthesis. To remedy this problem, we designed pGEMM7, where the two genes under SP6 promoter control were flipped in the opposite reading direction (**Supplementary Fig. 1**). As expected, expression of pGEMM7 resulted in no pgsA protein and no PG phospholipid production when the SP6 RNAP was omitted (main text **Fig. 1b,c**).

Supplementary Note 2: Absence of PgpA specific signal in MS data

We were not able to detect a suitable peptide for PgpA. Therefore, PgsA was used as a reporter of transcriptional activation of the PgsA-PgpA branch upon SP6 RNAP addition (main text **Fig. 1a,b**). As an alternative to PgpA, PgpC (Uniprot: P0AD42) can catalyze the same enzymatic reaction as PgpA. Four peptides of PgpC were detected with our protocol for trypsin digestion and LC-MS/MS as shown in **Supplementary Fig. 7**. They are listed in **Supplementary Table 5**.

Supplementary Note 3: Analysis of purified LactC2-mCherry by PAGE

The presence of two to three prominent bands of the LactC2-mCherry fusion protein observed in **Supplementary Fig. 12b** does not reflect a low purity. Instead, they correspond to different denaturation forms of LactC2-mCherry that migrate differently on gel. This observation has already been reported in the case of another mCherry fusion protein [3]. In their study, Mestrom et al. found that a stabilised form of the fusion protein was resistant to at least 2% SDS and ran at a lower apparent molecular weight by PAGE. This more native form of the fusion protein would correspond to one of the lower bands of LactC2-mCherry marked with a circle symbol in **Supplementary Fig. 12b**.

Further purification of LactC2-mCherry by gel filtration (Sephacryl S200 16/60 HiPrep mounted on an ÄKTA Pure system, both from GE Healthcare) failed to eliminate the extra bands visible by Coomassie staining (**Supplementary Fig. 13**, upper panel), indicating that they all correspond to the same protein.

Additionally, we analysed these LactC2-mCherry samples using anion exchange chromatography (MonoQ 4.6/100 PE column on an ÄKTA Pure system, GE Healthcare). Isolated samples were treated with 2 M urea and 95 °C for different periods of time, and were loaded on a 4-12% Bis-Tris SDS gel ran in MES buffer (**Supplementary Fig. 14**). The two prominent bands corresponding to fully and partially denatured states of the mCherry fusion protein can be observed. The middle one that is visible in the fluorescence channel disappeared after heat treatment, further indicating that it corresponds to a more folded, native form.

Concluding, the prominent bands observed in the lane of the purified LactC2-mCherry all correspond to the same protein and the level of purity is sufficient for utilisation as a reporter probe for PS lipids (**Supplementary Figs. 17** and **18**).

Supplementary Note 4: Kinetic analysis of LactC2-eGFP association to PS-producing liposomes

Phenomenological fitting was applied to extract kinetic parameters from the time traces reported in main text **Fig. 6b** (**Supplementary Fig. 19**). The following sigmoid equation was used:

$$y = k' + k\,\frac{t^n}{t^n + K^n} \qquad \text{(Eq. 1)}$$

Where *t* is the time in minutes, and *y* is the LactC2-eGFP fluorescence signal at the rim of a liposome at a given time point. *k*, *k'*, *K*, and *n* are fitting parameters. This equation has previously been used to fit fluorescence measurements of cell-free gene expression of YFP in liposomes [4], and mass spectrometry measurements of cell-free Min protein expression [5]. The plateau time, i.e. the time until LactC2-eGFP fluorescence stops increasing, was defined as:

$$T_{plateau} = \frac{2K}{n} + K. \qquad \text{(Eq. 2)}$$

The rate, which is the steepness at time $t = K$, was defined as:

$$\text{rate} = \frac{kn}{4K}. \qquad \text{(Eq. 3)}$$

This apparent rate captures the rate of transcription and translation, the enzyme kinetics leading to the synthesis of PS, the membrane incorporation of PS, as well as the binding kinetics of LactC2-eGFP to PS, as illustrated in **Supplementary Fig. 19a**.

SUPPLEMENTARY TABLES

Supplementary Table 1: List of plasmids used in this study

Plasmid	Size (kb)	Encoded genes
pGEMM7	10.5	*plsB*, *plsC*, *cdsA*, *pssA*, *psd*, *pgsA*, *pgpA*
pGEMM6	10.5	*plsB*, *plsC*, *cdsA*, *pssA*, *psd*, *pgsA*, *pgpA*
pUC57-T7p-LacO-meYFP-LL-spinach-T7t	3.8	*meYFP*
pUC57-SP6p-LacO-meYFP-LL-spinach-T7t	3.8	*meYFP*

Supplementary Table 2: List of primers used in this study

Primer	Sequence, 5' to 3'	Linker site	Target
25 ChD	GATGCTGTAGGCATAGGCTTGG		
91 ChD	AAAAAACCCCTCAAGACCCGTTTAGAGG		
288 ChD	CGATGCGTCCGGC		
310 ChD	GGATCTCGACGCTCTCCCTTATG		
397 ChD	CCTCTAGAAATAATTTTGTTTAACTTTAAGAAGG		
471 ChD	CAAAGCCCGAAAGGAAGCTGA		
507 ChD	ATGTATATCTCCTTCTTAAAGTTAAACAAAATTATTTCTAGAGG		pUC57
535 ChD	TAGCATAACCCCTTGGGGCCTCTAAAC		pUC57
628 ChD	TGGGCCCGTAACAAAATCCTCCCAATAAGCTAATACGACTCACTATAGG	1 top	*plsB*
629 ChD	ACCAGGGCTGTTCAACCGACGCTCACGGGGCAAAAAACCCCTCAAGACC	2 bottom	*plsB*
630 ChD	CCCCGTGAGCGTCGGTTGAACAGCCCTGGTTAATACGACTCACTATAGG	2 top	*plsC*
631 ChD	AGCGATATATTCGGGCTTCTGGTCGGGCCGCAAAAAACCCCTCAAGACC	3 bottom	*plsC*
632 ChD	CGGCCCGACCAGAAGCCCGAATATATCGCTTAATACGACTCACTATAGG	3 top	*cdsA*
633 ChD	AGGTAACGCACCCCGGCCCAAGAGCCGTAACAAAAAACCCCTCAAGACC	4 bottom	*cdsA*
634 ChD	TTACGGCTCTTGGGCCGGGGTGCGTTACCTTAATACGACTCACTATAGG	4 top	*pssA*
635 ChD	AGGAATTAACGGACGGCCTCGATTTCTGCACAAAAAACCCCTCAAGACC	5 bottom	*pssA*
636 ChD	TGCAGAAATCGAGGCCGTCCGTTAATTCCTTAATACGACTCACTATAGG	5 top	*psd*
715 ChD	GGAATTGTGAGCGGATAACAATTCCCCTCTAGAAATAATTTTGTTTAACTTT		
716 ChD	GAATTGTTATCCGCTCACAATTCCGGTCTCCCTATAGTGAGTCG		
719 ChD	ATTTAGGTGACACTATAGAAGAACCGGAATTGTGAGCGGA		
720 ChD	TCTTCTATAGTGTCACCTAAATATTTCGCATCTAGATGCATTCGC		
723 ChD	TCGATATTGGGGACTTCTCAAATCTCGTCACAAAAAACCCCTCAAGACC	SHR18 bottom	*psd*
848 ChD	TATACATATGGGCAGCAGCCATCATCATCATCATCACAGCAGCGGCCTGGTGCCGCGCG GCAGCCATATGGTGAGCAAGGGCGAGG		
849 ChD	AACTCAGCTTCCTTTCGGGCTTTGCTAACAGCCCAGCAGCTCC		
850 ChD	GATGATGGCTGCTGCCCATATGTATATCTCCTTCTTAAAGTTAAAC		
851 ChD	CCTGCAGGCCTTAGGCTCGAGCGGCCGCTGAGGACTAGTATTTAGGTGACACTATAGA	13 top	*pgpA*
852 ChD	TGACGAGATTTGAGAAGTCCCCAATATCGACAAAAAACCCCTCAAGACC	SHR18 top	*pgsA*
829 ChD	TGACGAGATTTGAGAAGTCCCCAATATCGAATTTAGGTGACACTATAGAAGAACCCCTCT AGAAATAATTTTGTTTAACTTTAAGAAGG	13 bottom	pUC19
830 ChD	GCTTATTGGGAGGATTTTGTTACGGGCCCAGAATCAGGGGATAACGCAGG	1 bottom	pUC19
818 ChD	GTGTCAGTCAATCACGGGCGGGTCCACTACCAAAAAACCCCTCAAGACCCGTTTAG	30 bottom	*pgpA*

819 ChD	GTAGTGGACCCGCCCGTGATTGACTGACACATTTAGGTGACACTATAGAAGAATCCCCT CTAGAAATAATTTTGTTTAAC	30 top	*pgsA*

Supplementary Table 3: Pipetting scheme of Gibson assembly to obtain pGEMM7

Part	Size (kb)	Ratio length to backbone	Mass DNA added into reaction (ng)
pUC19	2	1	100
pgpA	0.8	0.4	40
pgsA	0.8	0.4	40
plsB	2.6	1.3	130
plsC	0.9	0.45	45
cdsA	1.2	0.6	60
pssA	1.4	0.7	70
psd	1	0.5	50

Supplementary Table 4: Full list of the tryptic peptides detected by LC-MS/MS in this study. The first column shows the uniprot accession number as well as the gene name. The peptide sequence is shown in column 2 followed by the standard type used (internal for absolute quantification, global for normalization). The start and end positions of the peptide in the wild-type gene are indicated. In the last two columns, the predicted and measured retention time values are reported.

Protein (Uniprot No.)	Peptide	Standard type	Begin #AA	End #AA	Predicted retention time (min)	Average measured retention time (min)
PlsB (P0A7A7)	LLNLPLSILVK		10	20	17.87	20.31
PlsB (P0A7A7)	FSPSVSLR		166	173	7.77	8.09
PlsB (P0A7A7)	LAAVGPR		202	208	2.58	2.9
PlsB (P0A7A7)	DTIGDIIILPR	Internal standard	589	599	16.94	16.81
PlsC (P26647)	LAPLFGLK		44	51	13.66	13.48
PlsC (P26647)	GLLPFK		154	159	10.14	10.49
CdsA (P0ABG1)	DSGHLIPGHGGILDR		248	262	10.4	8.1
PssA (P23830)	GILNALYEAK		65	74	11.93	12.49
PssA (P23830)	DLQSIADYPVK	Internal standard	419	429	9.57	11
Psd (P0A8K1)	LSLQYILPK		6	14	13.64	14.89
Psd (P0A8K1)	LVIDLFVK		35	42	16.2	15.41
PgsA (P0ABF8)	EIIISALR		101	108	12.73	11.36
PgsA (P0ABF8)	SSVAVSWIGK	Internal standard	118	127	11.03	10.34
EF-Tu (P0CE47)	TTLTAAITTVLAK	Global standard	25	37	13.94	16.65
EF-Tu (P0CE47)	GITINTSHVEYDTPTR		59	74	9.11	9.56

Supplementary Table 5: Transitions of the MS/MS measurements for the proteomic analysis

Protein (Uniprot No.)	Peptide	Precursor ion *m/z*	MS1 Res	Product ion *m/z*	MS2 Res	Dwell time (ms)	Fragmentor (V)	Collision energy (V)	Ion
PlsB (P0A7A7)	LLNLPLSILVK	611.9103	Unit	769.5182	Unit	20	130	20	y7
PlsB (P0A7A7)	LLNLPLSILVK	611.9103	Unit	227.1754	Unit	20	130	20	b2
PlsB (P0A7A7)	LLNLPLSILVK	611.9103	Unit	341.2183	Unit	20	130	20	b3
PlsB (P0A7A7)	LLNLPLSILVK	611.9103	Unit	454.3024	Unit	20	130	20	b4
PlsB (P0A7A7)	FSPSVSLR	446.748	Unit	658.3883	Unit	20	130	14.8	y6
PlsB (P0A7A7)	FSPSVSLR	446.748	Unit	375.235	Unit	20	130	14.8	y3
PlsB (P0A7A7)	FSPSVSLR	446.748	Unit	288.203	Unit	20	130	14.8	y2
PlsB (P0A7A7)	FSPSVSLR	446.748	Unit	235.1077	Unit	20	130	14.8	b2
PlsB (P0A7A7)	LAAVGPR	342.2136	Unit	499.2987	Unit	20	130	11.6	y5
PlsB (P0A7A7)	LAAVGPR	342.2136	Unit	428.2616	Unit	20	130	11.6	y4
PlsB (P0A7A7)	LAAVGPR	342.2136	Unit	329.1932	Unit	20	130	11.6	y3
PlsB (P0A7A7)	LAAVGPR	342.2136	Unit	185.1285	Unit	20	130	11.6	b2
PlsB (P0A7A7)	DTIGDIIILPR	613.3612	Unit	896.5564	Unit	20	130	20	y8
PlsB (P0A7A7)	DTIGDIIILPR	613.3612	Unit	611.4239	Unit	20	130	20	y5
PlsB (P0A7A7)	DTIGDIIILPR	613.3612	Unit	498.3398	Unit	20	130	20	y4
PlsB (P0A7A7)	DTIGDIIILPR	613.3612	Unit	385.2558	Unit	20	130	20	y3
PlsB (P0A7A7)	DTIGDIIILPR	613.3612	Unit	272.1717	Unit	20	130	20	y2
PlsB (P0A7A7)	DTIGDIIILPR.heavy	618.3653	Unit	906.5646	Unit	20	130	20	y8
PlsB (P0A7A7)	DTIGDIIILPR.heavy	618.3653	Unit	621.4322	Unit	20	130	20	y5
PlsB (P0A7A7)	DTIGDIIILPR.heavy	618.3653	Unit	508.3481	Unit	20	130	20	y4
PlsB (P0A7A7)	DTIGDIIILPR.heavy	618.3653	Unit	395.264	Unit	20	130	20	y3
PlsB (P0A7A7)	DTIGDIIILPR.heavy	618.3653	Unit	282.18	Unit	20	130	20	y2
PlsC (P26647)	LAPLFGLK	429.776	Unit	674.4236	Unit	20	130	14.3	y6
PlsC (P26647)	LAPLFGLK	429.776	Unit	464.2867	Unit	20	130	14.3	y4
PlsC (P26647)	LAPLFGLK	429.776	Unit	337.7154	Unit	20	130	14.3	y6
PlsC (P26647)	LAPLFGLK	429.776	Unit	185.1285	Unit	20	130	14.3	b2
PlsC (P26647)	GLLPFK	337.7154	Unit	504.318	Unit	20	130	11.5	y4
PlsC (P26647)	GLLPFK	337.7154	Unit	391.234	Unit	20	130	11.5	y3

PlsC (P26647)	GLLPFK	337.7154	Unit	171.1128	Unit	20	130	11.5	b2
PlsC (P26647)	GLLPFK	337.7154	Unit	284.1969	Unit	20	130	11.5	b3
CdsA (P0ABG1)	DSGHLIPGHGGILDR	515.2707	Unit	630.3570	Unit	20	130	8.15	Y6
CdsA (P0ABG1)	DSGHLIPGHGGILDR	515.2707	Unit	397.1466	Unit	20	130	8.15	b4
CdsA (P0ABG1)	DSGHLIPGHGGILDR	515.2707	Unit	510.2306	Unit	20	130	8.15	b5
CdsA (P0ABG1)	DSGHLIPGHGGILDR	515.2707	Unit	623.3147	Unit	20	130	8.15	b6
PssA (P23830)	GILNALYEAK	546.3084	Unit	921.504	Unit	20	130	17.9	y8
PssA (P23830)	GILNALYEAK	546.3084	Unit	808.4199	Unit	20	130	17.9	y7
PssA (P23830)	GILNALYEAK	546.3084	Unit	623.3399	Unit	20	130	17.9	y5
PssA (P23830)	DLQSIADYPVK	624.8272	Unit	892.4775	Unit	20	130	20.4	y8
PssA (P23830)	DLQSIADYPVK	624.8272	Unit	692.3614	Unit	20	130	20.4	y6
PssA (P23830)	DLQSIADYPVK	624.8272	Unit	506.2973	Unit	20	130	20.4	y4
PssA (P23830)	DLQSIADYPVK	624.8272	Unit	357.1769	Unit	20	130	20.4	b3
PssA (P23830)	DLQSIADYPVK.heavy	628.8343	Unit	900.4917	Unit	20	130	20.4	y8
PssA (P23830)	DLQSIADYPVK.heavy	628.8343	Unit	700.3756	Unit	20	130	20.4	y6
PssA (P23830)	DLQSIADYPVK.heavy	628.8343	Unit	514.3115	Unit	20	130	20.4	y4
PssA (P23830)	DLQSIADYPVK.heavy	628.8343	Unit	357.1769	Unit	20	130	20.4	b3
Psd (P0A8K1)	LSLQYILPK	537.8315	Unit	633.397	Unit	20	130	17.7	y5
Psd (P0A8K1)	LSLQYILPK	537.8315	Unit	357.2496	Unit	20	130	17.7	y3
Psd (P0A8K1)	LSLQYILPK	537.8315	Unit	244.1656	Unit	20	130	17.7	y2
Psd (P0A8K1)	LSLQYILPK	537.8315	Unit	831.4975	Unit	20	130	17.7	b7
Psd (P0A8K1)	LVIDLFVK	473.8022	Unit	833.5131	Unit	20	130	15.7	y7
Psd (P0A8K1)	LVIDLFVK	473.8022	Unit	734.4447	Unit	20	130	15.7	y6
Psd (P0A8K1)	LVIDLFVK	473.8022	Unit	506.3337	Unit	20	130	15.7	y4
Psd (P0A8K1)	LVIDLFVK	473.8022	Unit	213.1598	Unit	20	130	15.7	b2
PgsA (P0ABF8)	EIIISALR	457.7871	Unit	559.3562	Unit	20	130	15.2	y5
PgsA (P0ABF8)	EIIISALR	457.7871	Unit	446.2722	Unit	20	130	15.2	y4
PgsA (P0ABF8)	EIIISALR	457.7871	Unit	359.2401	Unit	20	130	15.2	y3
PgsA (P0ABF8)	EIIISALR	457.7871	Unit	356.218	Unit	20	130	15.2	b3
PgsA (P0ABF8)	SSVAVSWIGK	517.2875	Unit	760.4352	Unit	20	130	17	y7
PgsA (P0ABF8)	SSVAVSWIGK	517.2875	Unit	689.3981	Unit	20	130	17	y6

PgsA (P0ABF8)	SSVAVSWIGK	517.2875	Unit	590.3297	Unit	20	130	17	y5
PgsA (P0ABF8)	SSVAVSWIGK	517.2875	Unit	345.1769	Unit	20	130	17	b4
PgsA (P0ABF8)	SSVAVSWIGK.heavy	521.2946	Unit	768.4494	Unit	20	130	17	y7
PgsA (P0ABF8)	SSVAVSWIGK.heavy	521.2946	Unit	697.4123	Unit	20	130	17	y6
PgsA (P0ABF8)	SSVAVSWIGK.heavy	521.2946	Unit	598.3439	Unit	20	130	17	y5
PgsA (P0ABF8)	SSVAVSWIGK.heavy	521.2946	Unit	345.1769	Unit	20	130	17	b4
EF-TU (P0CE47)	TTLTAAITTVLAK	652.3952	Unit	887.556	Unit	20	130	21.2	y9
EF-TU (P0CE47)	TTLTAAITTVLAK	652.3952	Unit	816.5189	Unit	20	130	21.2	y8
EF-TU (P0CE47)	TTLTAAITTVLAK	652.3952	Unit	745.4818	Unit	20	130	21.2	y7
EF-TU (P0CE47)	TTLTAAITTVLAK	652.3952	Unit	632.3978	Unit	20	130	21.2	y6
EF-TU (P0CE47)	GITINTSHVEYDTPTR	601.9672	Unit	752.3573	Unit	20	130	16.9	y6
EF-TU (P0CE47)	GITINTSHVEYDTPTR	601.9672	Unit	474.2671	Unit	20	130	16.9	y4
EF-TU (P0CE47)	GITINTSHVEYDTPTR	601.9672	Unit	710.3286	Unit	20	130	16.9	y12
EF-TU (P0CE47)	GITINTSHVEYDTPTR	601.9672	Unit	187.1133	Unit	20	130	16.9	y3
PgpC (P0AD42)	LQTLQADFVR	595.8300	Unit	949.5101	Unit	20	130	10.12	y8
PgpC (P0AD42)	LQTLQADFVR	595.8300	Unit	735.3784	Unit	20	130	10.12	y6
PgpC (P0AD42)	LQTLQADFVR	595.8300	Unit	242.1499	Unit	20	130	10.12	b2
PgpC (P0AD42)	LQTLQADFVR	595.8300	Unit	343.1975	Unit	20	130	10.12	b3
PgpC (P0AD42)	DNVTAFPLVQER	694.8620	Unit	959.5308	Unit	20	130	12.04	y8
PgpC (P0AD42)	DNVTAFPLVQER	694.8620	Unit	888.4937	Unit	20	130	12.04	y7
PgpC (P0AD42)	DNVTAFPLVQER	694.8620	Unit	741.4253	Unit	20	130	12.04	y6
PgpC (P0AD42)	DNVTAFPLVQER	694.8620	Unit	230.0771	Unit	20	130	12.04	b2
PgpC (P0AD42)	VNLIASQIQR	571.3380	Unit	631.3521	Unit	20	130	8.29	y5
PgpC (P0AD42)	VNLIASQIQR	571.3380	Unit	303.1775	Unit	20	130	8.29	y2
PgpC (P0AD42)	VNLIASQIQR	571.3380	Unit	214.1186	Unit	20	130	8.29	b2
PgpC (P0AD42)	VNLIASQIQR	571.3380	Unit	440.2867	Unit	20	130	8.29	b4
PgpC (P0AD42)	GYGGWVLTMR	570.2869	Unit	919.4818	Unit	20	130	13	y8
PgpC (P0AD42)	GYGGWVLTMR	570.2869	Unit	520.2911	Unit	20	130	13	y4
PgpC (P0AD42)	GYGGWVLTMR	570.2869	Unit	407.2071	Unit	20	130	13	y3
PgpC (P0AD42)	GYGGWVLTMR	570.2869	Unit	221.0920	Unit	20	130	13	b2

Supplementary Table 6: Mass spectrometry detection settings for phospholipid detection. Measurements in positive and negative modes were performed separately to circumvent polarity switching. Asterisk (*) indicates species incorporating ^{13}C-G3P, resulting in a 3 Da mass shift with respect to the regular species (6 Da for PG). Fragmentor voltage and collision energy were adapted from [6]. Novel species were assigned values of similar species. PGP products were not successfully detected. However, the transitions were scanned in all measurements and are therefore included here for completeness. Cell accelerator voltage was 4 V in all conditions.

Compound class	Compound name	Precursor ion *m/z*	Product ion *m/z*	Fragmentor (V)	Collision energy (eV)	Polarity
Matrix	DOPE	742.5	281.2	140	25	Negative
Matrix	DOPG	773.5	281.2	190	37	Negative
Matrix	Cardiolipin	727.5	281.2	140	29	Negative
Standards	DPPE	690.5	255.1	230	37	Negative
Standards	DPPG	721.5	255.1	220	45	Negative
Standards	POPE	716.5	281.2 255.1	140 230	25 37	Negative
Standards	POPG	750.5	281.2 255.1	190 220	37 45	Negative Negative
Standards	DOPS	786.5	281.2	130	40	Negative
16:0-product	16:0-LPA*	412.2	155.9	150	13	Negative
16:0-product	DPPA*	650.5	255.1	210	33	Negative
16:0-product	CDP-DPG*	955.5	712.4	135	55	Negative
16:0-product	DPPS*	737.5	255.1	180	41	Negative
16:0-product	DPPE*	693.5	255.1	230	37	Negative
16:0-product	DPPGP*	808	255.1	220	45	Negative
16:0-product	DPPG*	727.5	255.1	220	45	Negative
18:1-product	18:1-LPA*	438.3	155.9	160	17	Negative
18:1-product	DOPA*	702.5	281.2	190	37	Negative
18:1-product	CDP-DOG*	1007.5	764.5	135	55	Negative
18:1-product	DOPS*	789.5	281.2	130	40	Negative
18:1-product	DOPE*	745.5	281.2	140	25	Negative
18:1-product	DOPGP*	860	281.2	190	50	Negative
18:1-product	DOPG*	779.5	281.2	190	37	Negative
Mixed product	POPA*	676.5	281.2 255.1	190 210	37 33	Negative Negative
Mixed product	CDP-POG*	981.5	738.5	135	55	Negative

Mixed product	POPS*	763.5	281.2 255.1	130 180	40 41	Negative Negative
Mixed product	POPE*	719.5	281.2 255.1	140 230	25 37	Negative Negative
Mixed product	POPGP*	834	281.2 255.1	190 220	50 45	Negative Negative
Mixed product	POPG*	753.5	281.2 255.1	190 220	37 45	Negative Negative

Supplementary Table 7: Overview of synthesized lipid species. Symbols between square brackets correspond to residues as defined in the scheme below. Each species is a combination of two acyl chain residues (in numbers) and one head group residue (letter). Lipid species in bold have been quantitatively measured. Species in italic have not been unambiguously detected; however, their presence can be deduced from the successful measurements of subsequent reaction products.

Enzymes / Precursors	PlsB	PlsC	CdsA	PssA	Psd	PgsA	PgpA
Palmitoyl-CoA	16:0-LPA <2,1,a>	DPPA <2,2,a>	*CDP-DPG* <2,2,b>	DPPS <2,2,c>	**DPPE** <2,2,d>	*DPPGP* <2,2,e>	**DPPG** <2,2,f>
Oleoyl-CoA	18:1-LPA <3,1,a>	DOPA <3,3,a>	*CDP-DOG* <3,3,b>	DOPS <3,3,c>	**DOPE** <3,3,d>	*DOPGP* <3,3,e>	**DOPG** <3,3,f>
Palmitoyl-CoA + Oleoyl-CoA	16:0-LPA <2,1,a> 18:1-LPA <3,1,a>	DPPA <2,2,a> DOPA <3,3,a> POPA <2,3,a>, <3,2,a>	*CDP-DPG* <2,2,b> *CDP-DOG* <3,3,b> *CDP-POG* <2,3,b>, <3,2,b>	DPPS <2,2,c> DOPS <3,3,c> POPS <2,3,c>, <3,2,c>	**DPPE** <2,2,d> **DOPE** <3,3,d> **POPE** <2,3,d>, <3,2,d>	*DPPGP* <2,2,e> *DOPGP* <3,3,e> *POPGP* <2,3,e>, <3,2,e>	**DPPG** <2,2,f> **DOPG** <3,3,f> **POPG** <2,3,f>, <3,2,f>
Palmitoyl-CoA + NBD-palmitoyl-CoA	16:0-LPA <2,1,a> *NBD-LPA* <4,1,a>	DPPA <2,2,a> NBD-PPA <2,4,a>, <4,2,a> *NBD-NDB-PA* <4,4,a>	*CDP-DPG* <2,2,b> *CDP-NBD-PG* <2,4,b>, <4,2,b> *CDP-NBD-NBD-G* <4,4,b>	DPPS <2,2,c> NBD-PPS <2,4,c>, <4,2,c> *NBD-NDB-PS* <4,4,c>	**DPPE** <2,2,d> NBD-PPE <2,4,d>, <4,2,d> *NBD-NDB-PA* <4,4,d>	-	-

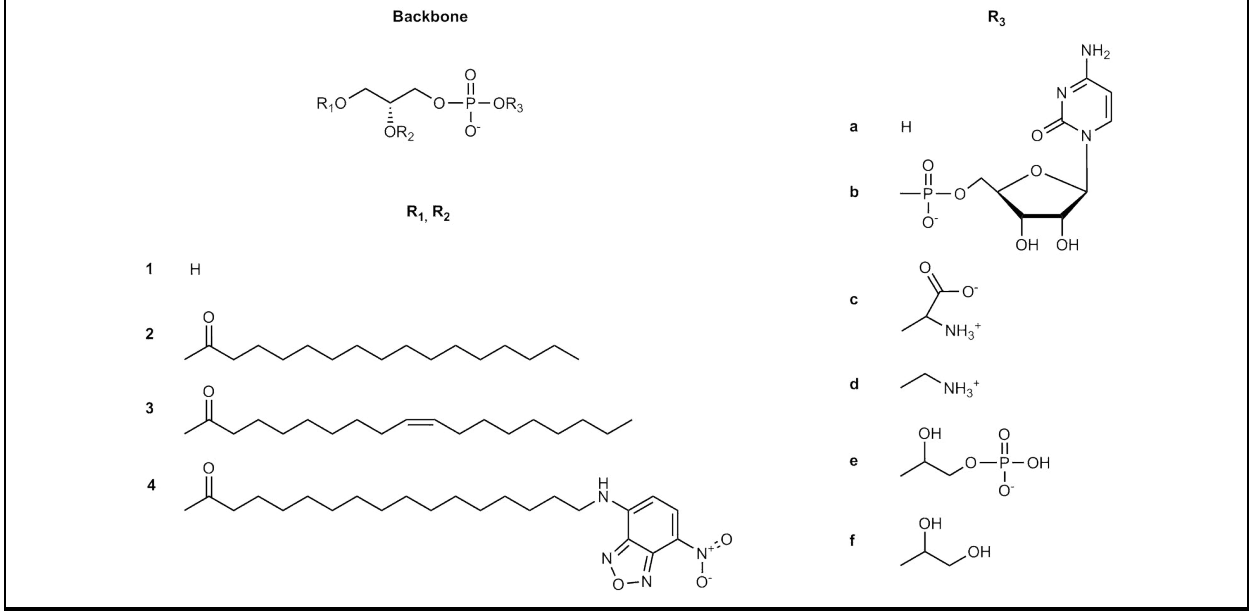

SUPPLEMENTARY FIGURES

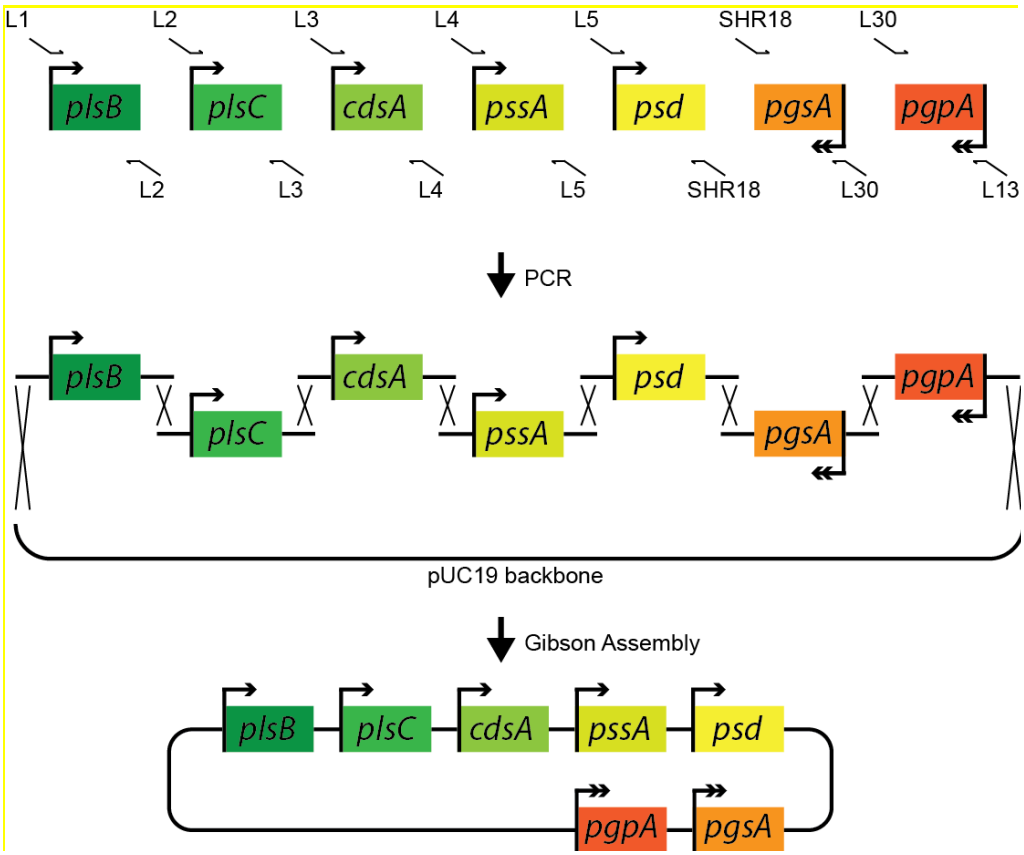

Supplementary Figure 1: Scheme for the construction of the pGEMM7 plasmid. Homologous linker sites are added to the transcriptional cassettes via PCR in the first step. After purification of the PCR fragments the entire plasmid is assembled by Gibson assembly in a single reaction.

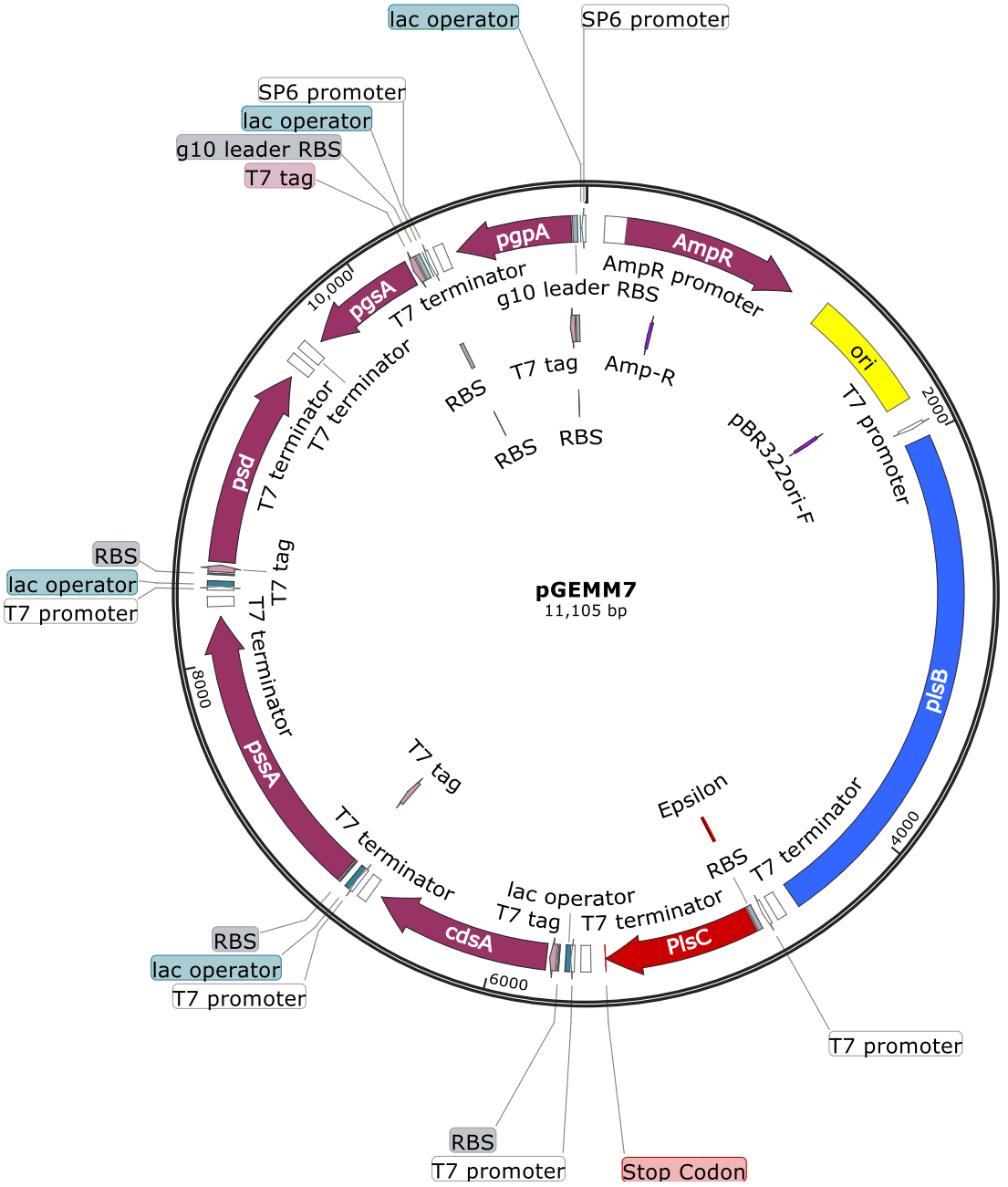

Supplementary Figure 2: Sequence map of the pGEMM7 construct. The plasmid map was generated with Snapgene.

a

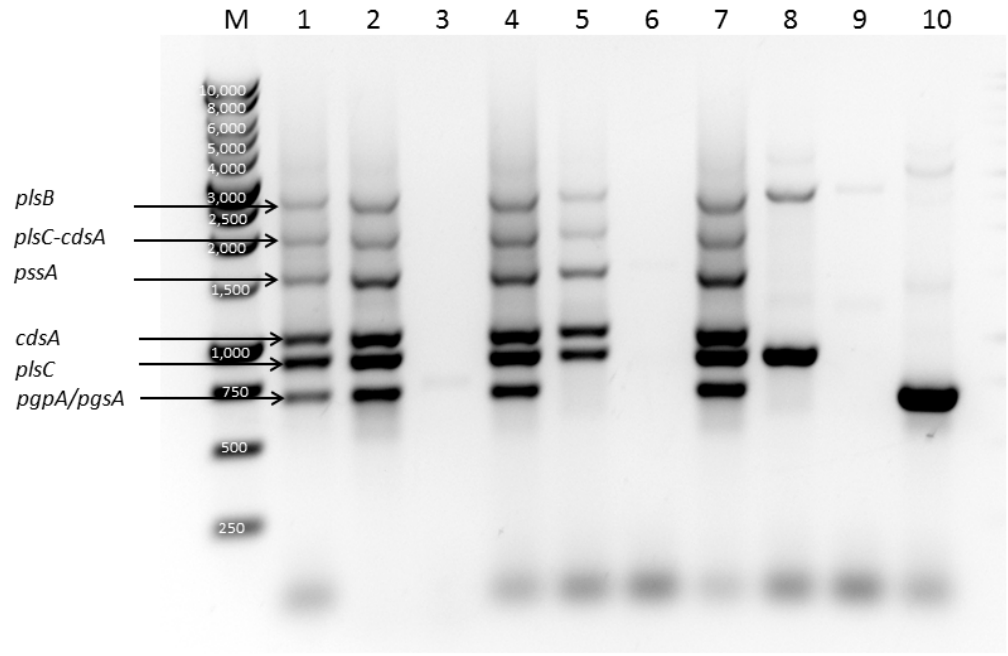

b

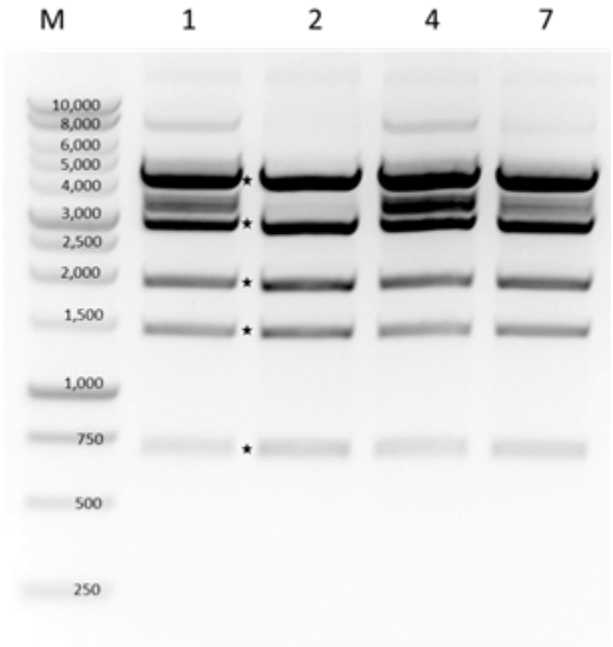

Supplementary Figure 3: Verification of pGEMM7 construct. a, Agarose gel of a colony PCR using primers 91 and 397. Colonies 1, 2, 4 and 7 were chosen to be further analysed due to the observed band pattern. First lane is the marker size. **b**, Agarose gel stained with SYBR safe DNA dye of a restriction digestion of pGEMM7. 1 µg of total DNA was loaded. 5 µL of Benchtop 1-kb ladder (Promega) were loaded in the first lane. The stars indicate the location of the expected bands. The numbers above the lanes indicate the colony number that was tested. These experiments were performed once.

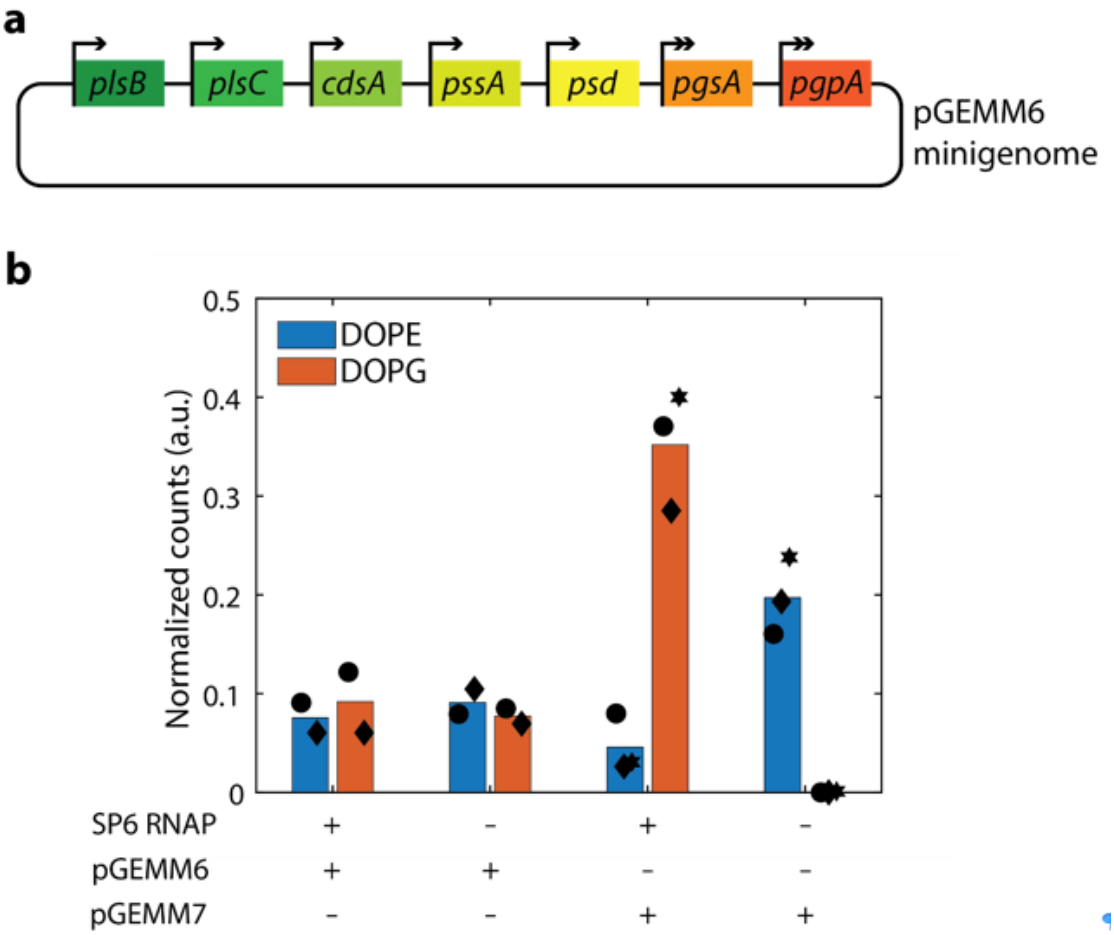

Supplementary Figure 4: Read-through causes non-specific PG synthesis with pGEMM6. a, Schematic representation of the pGEMM6 plasmid where all five genes under T7 promoter control (singel arrow) were assembled in the same orientation as the two genes *pgsA* and *pgpA* under SP6 promoter control (depicted by the double arrow). **b**, Synthesis of phospholipids from pGEMM6 (data with pGEMM7 are appended for comparison), in the presence of LUVs and all necessary precursors, with and without SP6 RNAP. The integrated peak intensity of ^{13}C-labelled lipids has been normalized to the signal of ^{12}C-DOPE to account for differences in MS sensitivity. In the absence of SP6 RNAP, *pgsA* and *pgpA* should not be expressed, and therefore, no DOPG should be synthesized. However, an appreciable yield of DOPG was observed without SP6 RNAP in the case of pGEMM6. We hypothesized that this was caused by transcription termination read-through by the T7 RNAP, transcribing downstream PG synthesis genes even if those are under control of an orthogonal promoter. This finding prompted us to design the new construct pGEMM7, where the two sets of PE and PG pathway genes were cloned in opposite directions to ensure full orthogonality. Bars are average values from two independent repeats (three with pGEMM7), each represented by a different symbol. Source Data are available for panel **b**.

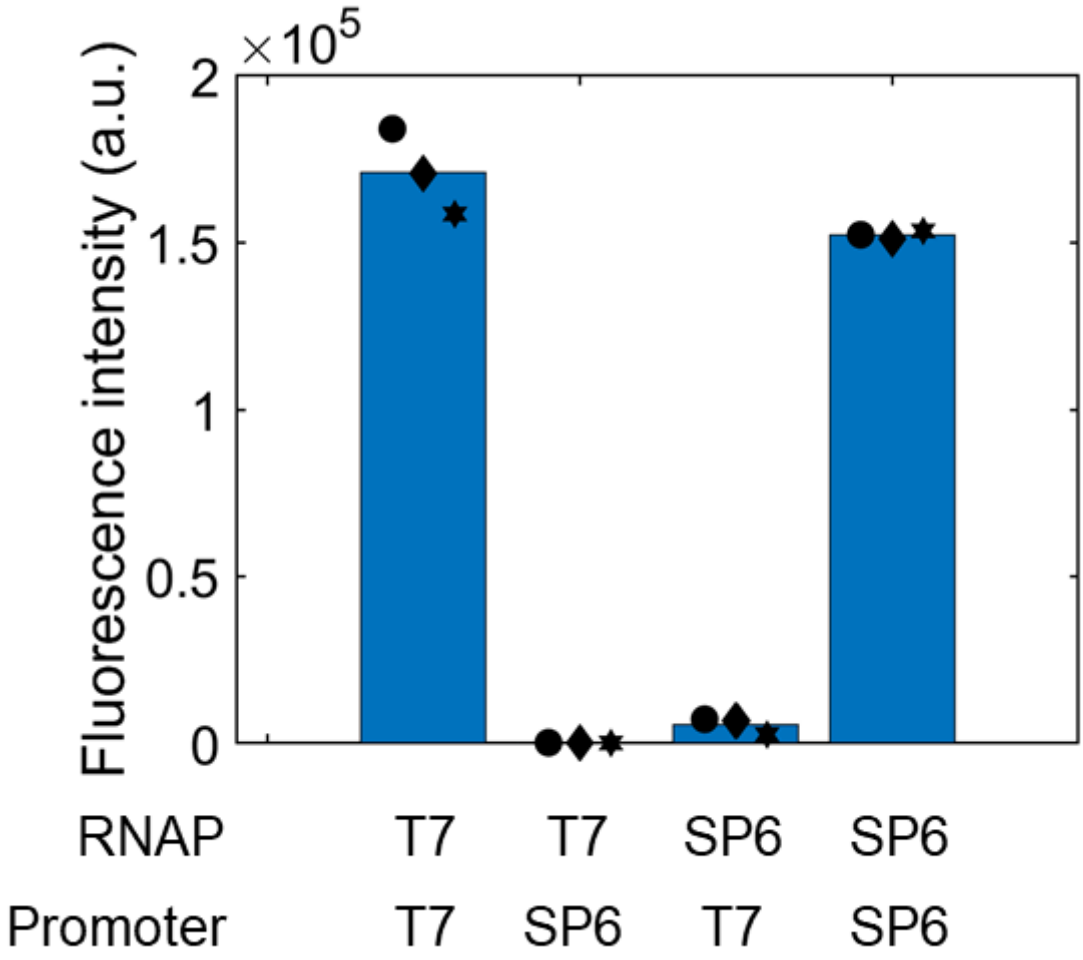

Supplementary Figure 5: Orthogonality diagram of T7 vs Sp6 promoters. The pUC57-T7p-LacO-meYFP-LL-spinach-T7t and pUC57-SP6p-LacO-meYFP-LL-spinach-T7t were expressed in PURE*frex*2.0 (ΔT7 RNAP) supplemented with either the T7 or SP6 RNAP. High end-point fluorescence signal from YFP was only observed with the canonical promoter/RNAP pairs, demonstrating strong orthogonality. Bars represent mean values from three repeats and the different symbols are individual data points. Source Data are available.

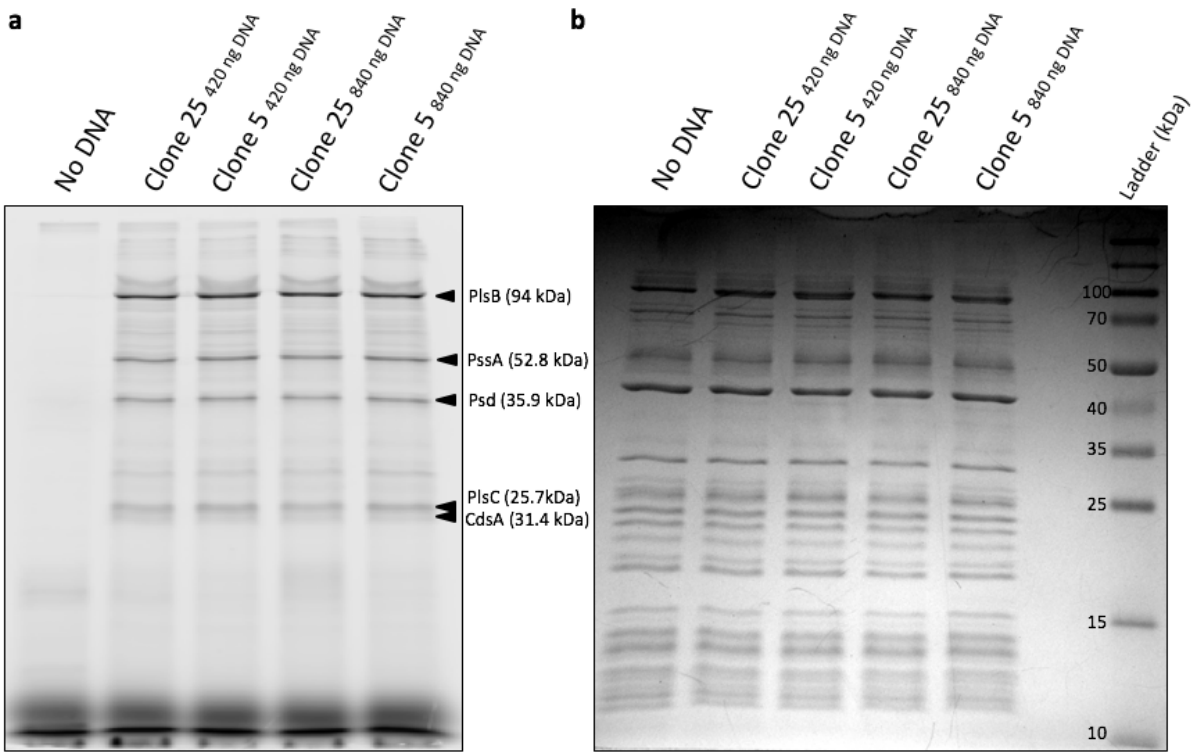

Supplementary Figure 6: Co-translational labelling of proteins with GreenLys. Early versions of pGEMM6 and pGEMM7 were screened for their ability to produce lipid-synthesizing enzymes. Clones 5 and 25 encode five genes that were successfully expressed in PURE*frex*2.0 supplemented with 1 µL of GreenLys reagent (Promega). The translation products were analysed by SDS-PAGE and Typhoon imaging. **a**, Fluorescence image with appended arrows pointing to the relevant protein bands. The protein names and theoretical molecular masses are indicated. Note that CdsA migrates significantly lower than predicted in the gel, as previously reported [6]. **b**, CBB stain image of the gel shown in a. Background proteins from the PURE system are visible, whereas the yield of synthesized proteins is too low to be directly observed. These experiments were performed once.

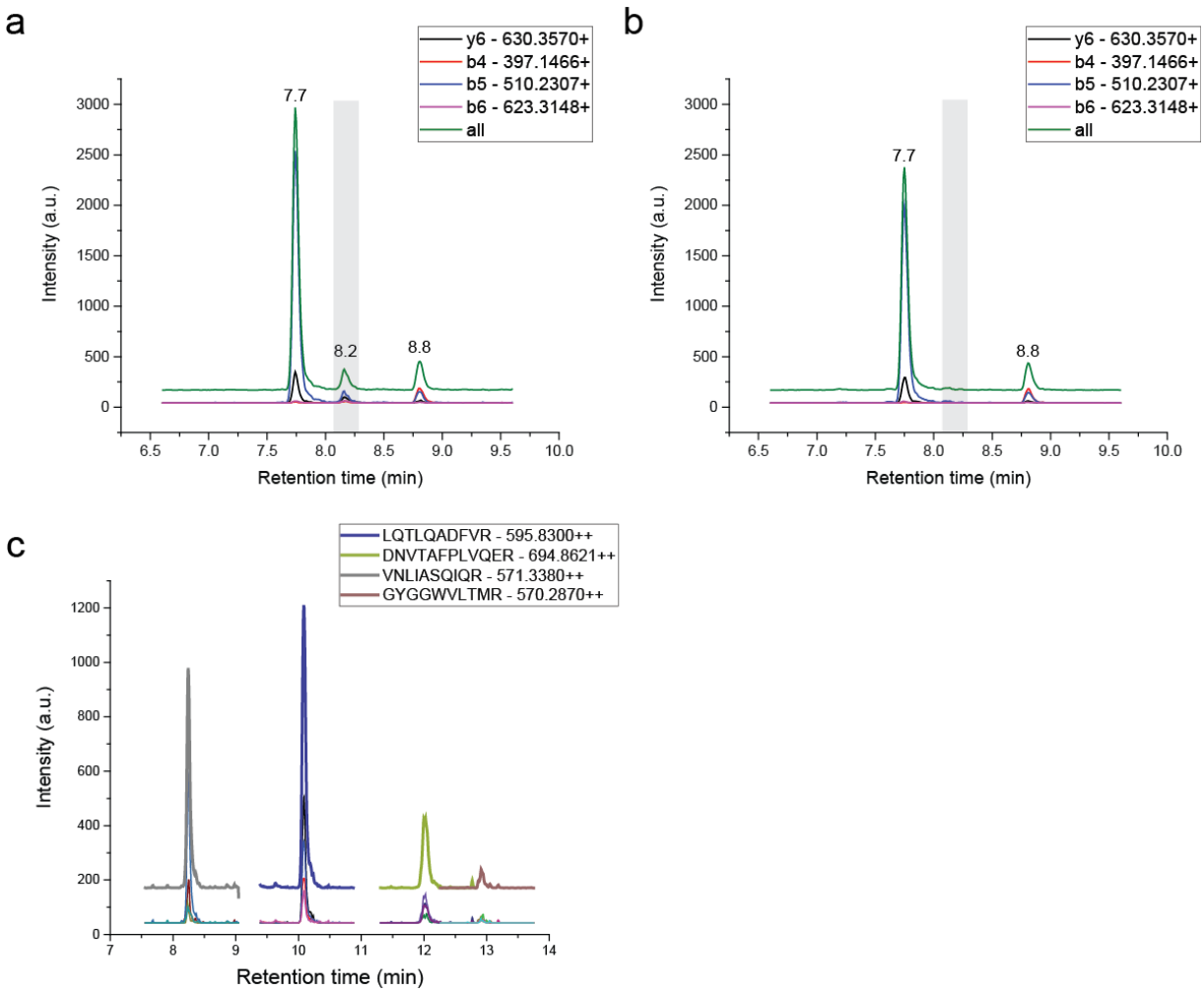

Supplementary Figure 7: LC-MS detection of CdsA by a single specific peptide DSGHLIPGHGGILDR and PgpC by four peptides. Peaks corresponding to tryptic peptides of the other enzymes were clearly identified and the chromatograms are not shown here. Their specifications can be found in **Supplementary Table 4**. **a**, Plotted intensities of four fragments of the CdsA peptide together with the combined intensities of all fragments. The overlayed gray area indicates the expected position at 8.2 min of the specific peak in the chromatogram. This specific peak is absent in a control cell-free protein expression reaction incubated without DNA (**b**). The visible peaks at 7.7 min and 8.8 min retention times can be attributed to background signals from the PURE*frex*2.0 proteins themselves or other contaminants. **c**, Chromatograms of all transitions and the combined measured ion current of each peptide of PgpC that were detectable after trypsin digestion. Source Data are available for panels **a** and **b**.

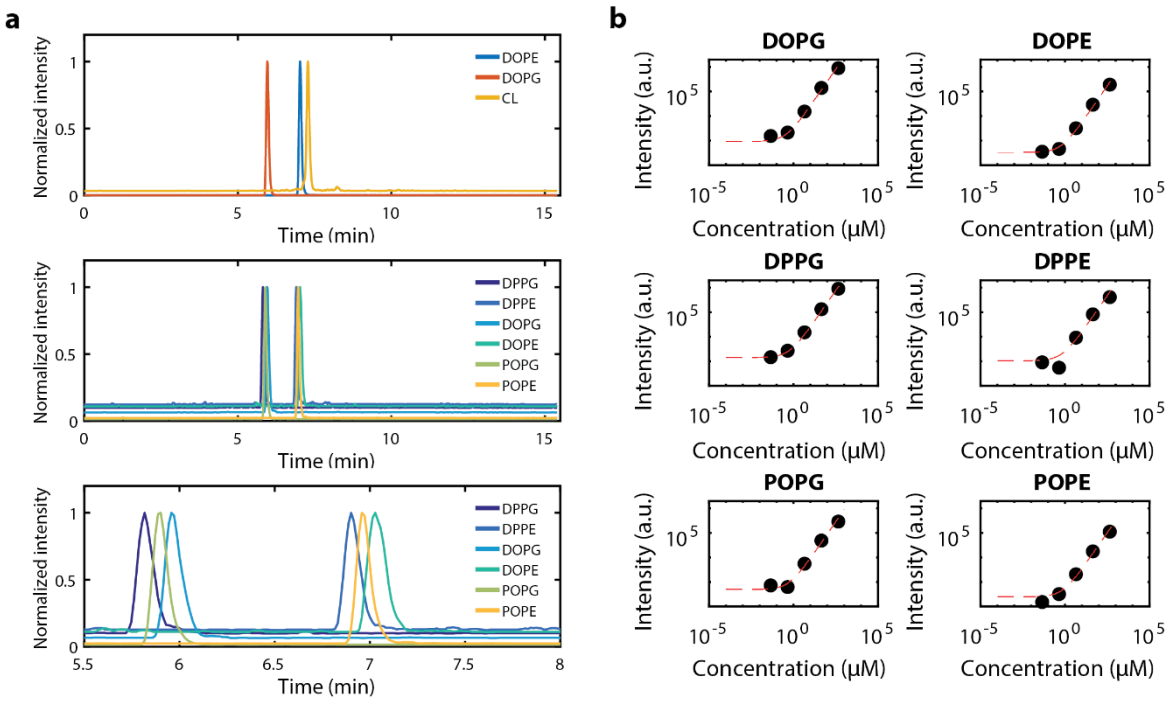

Supplementary Figure 8: LC-MS detection of phospholipids. a, Representative LC chromatograms of the studied phospholipids. Experimental conditions are as described in **Fig. 1c**. Two AU of SP6 RNAP, along with a 1:1 mix of oleoyl- and palmitoyl-CoA were supplemented to LUVs. Peak intensity was normalized to aid visualization. (top) Chromatograms of the lipids present in the liposome matrix. (middle, bottom) Chromatograms of synthesized phospholipids. The lower panel is a zoom-in graph, showing the typical elution pattern. Species with longer (oleoyl) chains elute later than species with shorter (palmitoyl) chains. **b**, Representative calibration curves for quantification of phospholipid concentrations. Five different known concentrations of the indicated phospholipids were injected, from low to high concentration, and plotted versus the resulting total integrated counts (TIC) of the corresponding peak labelled as 'Intensity' on the graphs. A linear fit was computed to obtain a calibration curve for each lipid (overlaid red dashed line). TIC values from cell-free synthesized lipids were then converted into absolute concentrations. Source Data are available for panel **b**.

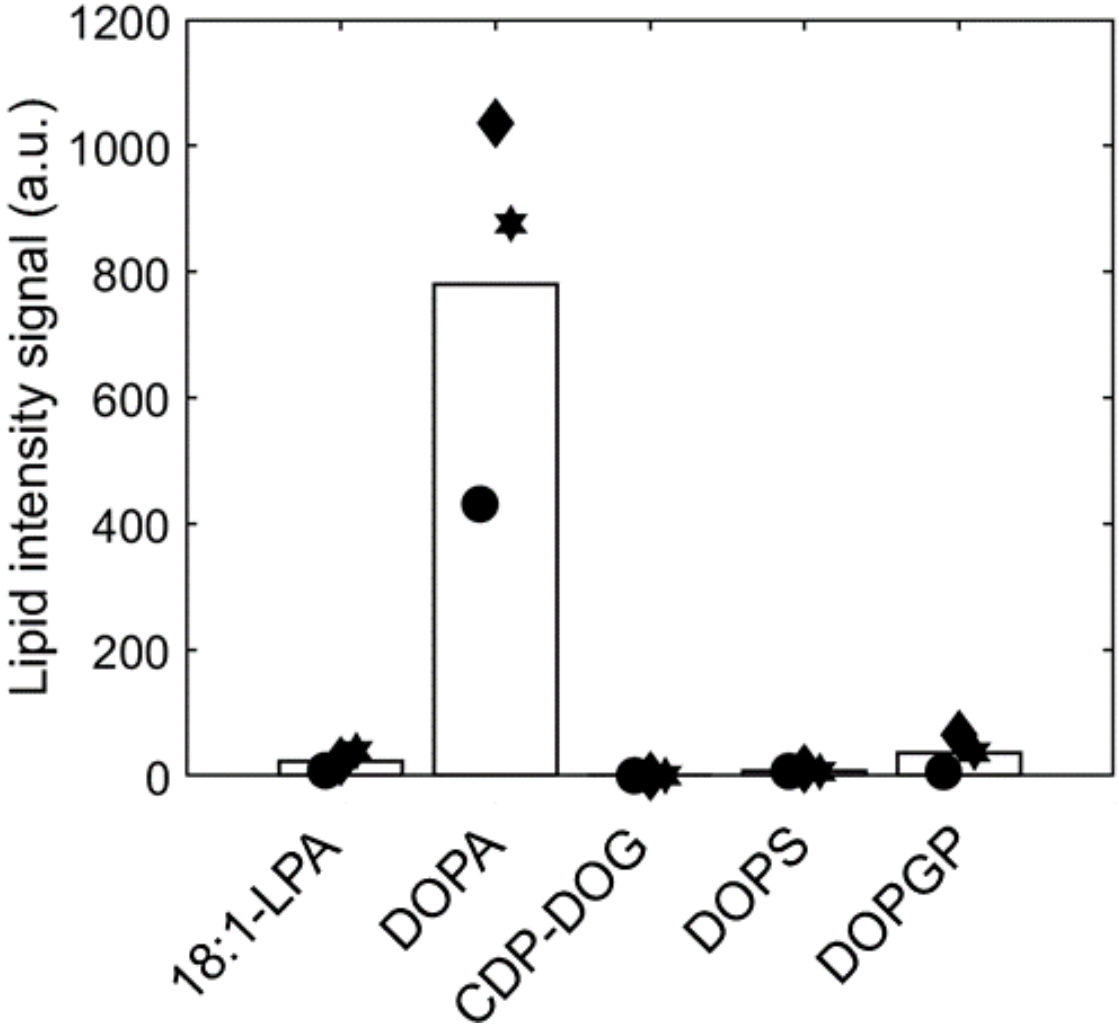

Supplementary Figure 9: Accumulation of lipid synthesis intermediates. Signal corresponding to all five lipid synthesis intermediate species. The measurements correspond to the rightmost data points shown in **Fig. 1c**, that is expression of pGEMM7 in the presence of LUVs and 4 AU of SP6 RNAP. Only DOPA accumulates in significant amounts. Other species have a total integrated peak intensity below 100 a.u.; therefore, the signals cannot be distinguished from noise. Source Data are available.

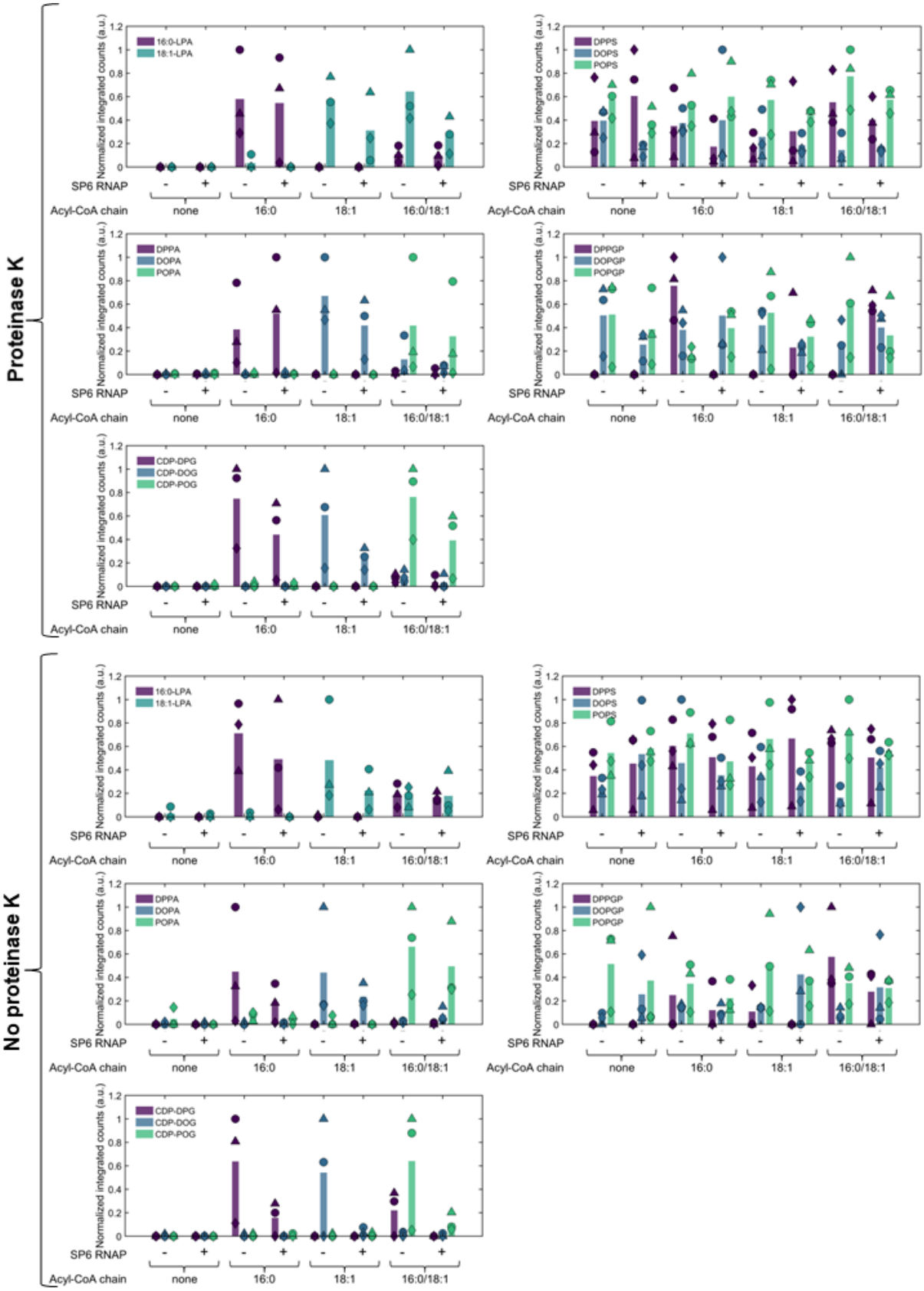

Supplementary Figure 10: LC-MS detection of synthesized phospholipids and accumulated intermediate products in giant liposome experiments. Phospholipid intermediates LPA, PA, and CDP-

DAG, but not PGP and PS, were detected. Data are plotted as total integrated counts normalized to the highest value per species, for all intermediate lipid species. Dataset was obtained from the same samples as shown in main text **Fig. 3d,e**. Bars indicate mean values. Symbols indicate values from individual experiments and correspond to data shown main text **Fig. 3d,e**. Precursors palmitoyl-CoA (16:0 acyl-CoA) and oleoyl-CoA (18:1 acyl-CoA) were used as indicated. Addition of proteinase K in the external medium confines gene expression to the interior of liposomes (upper panels). For LPAs, PAs and CDP-DAGs, signals were observed as expected, i.e. di-palmitoyl (DP) or di-oleoyl (DO) products when starting with 16:0 or 18:1 acyl-CoA, respectively, and both DP, DO and mixed chain products (PO) when starting with a mixture of the two precurscors. For PS and PGP species, no clear pattern was detected and only very low peak intensities (< 100 integrated counts) were measured. Because successful detection of PS was confirmed in other experiments (**Supplementary Fig. 16**), the results indicate that PS species do not accumulate under these conditions. In contrast, PGP signal was never observed, suggesting that its detection requires optimized protocols. Accumulation of LPAs, PAs, and CDP-DAGs was lower in the presence of SP6 RNAP when the PG synthesis pathway is active. Presumably, having two downstream pathways instead of one might result in a higher flux through the upstream (pre-branchpoint) part of the pathway. Source Data are available.

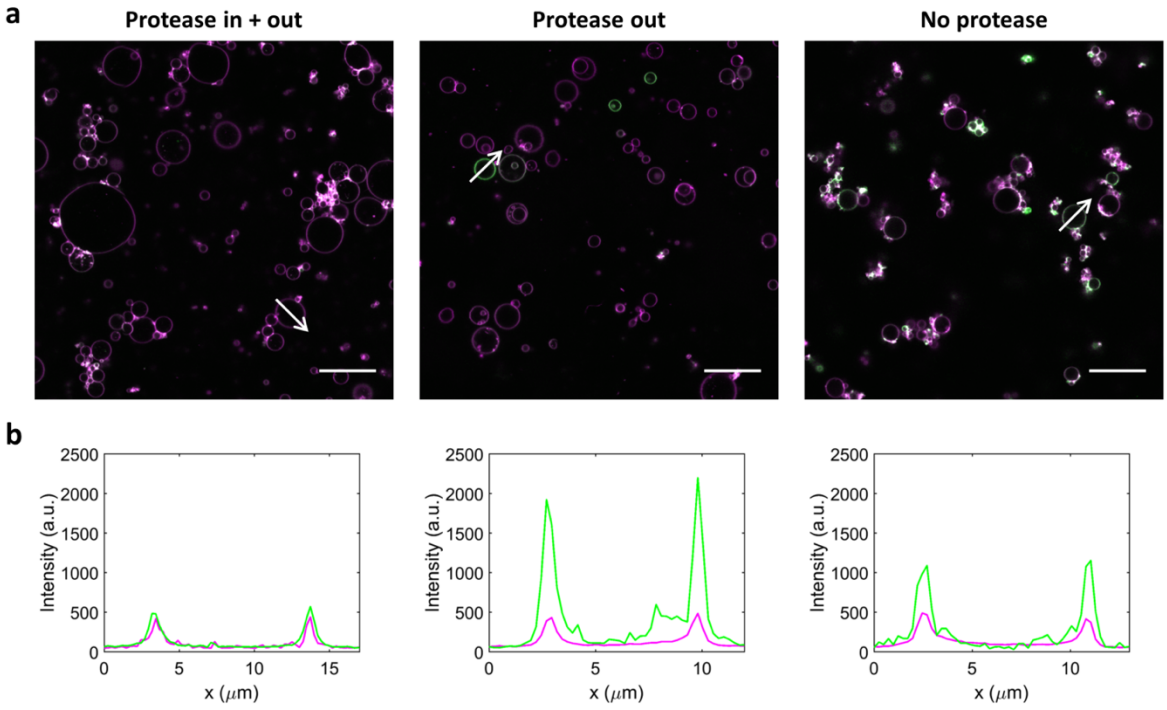

Supplementary Figure 11: Confocal fluorescence images of giant liposomes with synthesized NBD-labelled phospholipids. Experimental conditions are as indicated in main text **Fig. 4d**. Briefly, liposomes encapsulating pGEMM7 and PURE*frex*2.0 were prepared and incubated in the presence of NBD-palmitoyl-CoA and palmitoyl-CoA (1:9 mol. fraction). **a**, Representative images of different liposome samples are shown. Proteinase K was co-encapsulated inside liposomes, preventing gene expression and thus lipid synthesis (left). Proteinase K was added to preformed liposomes, preventing lipid synthesis from occurring outside the liposome lumina (middle). When no proteinase K was supplemented, gene expression and lipid synthesis can take place both inside and outside liposomes (right). All experimental conditions were tested three times and identical results were obtained. NBD fluorescence is shown in green and the Texas Red-dyed liposome membrane in magenta. Scale bars represent 20 µm. **b**, Line profiles of Texas Red (red) and NBD (green) signals along the arrows appended in **a**. a.u., arbitrary unit.

a

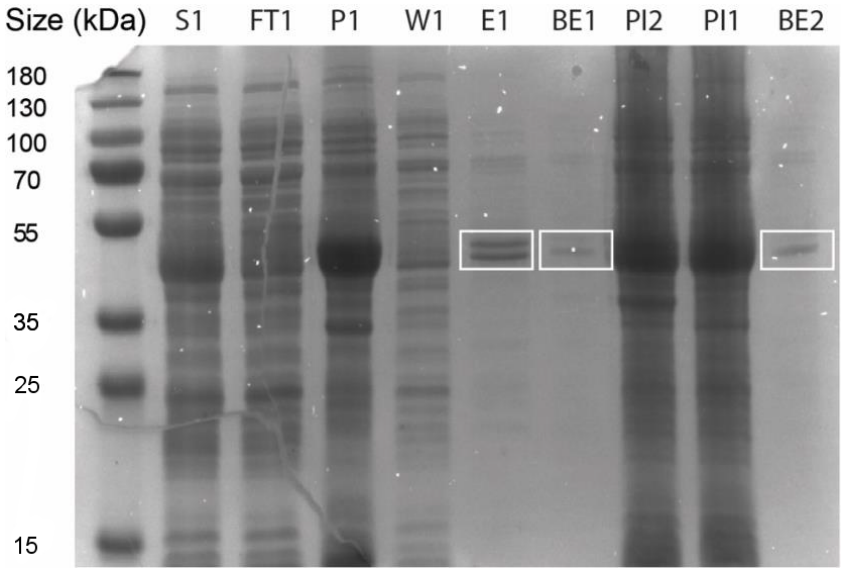

b

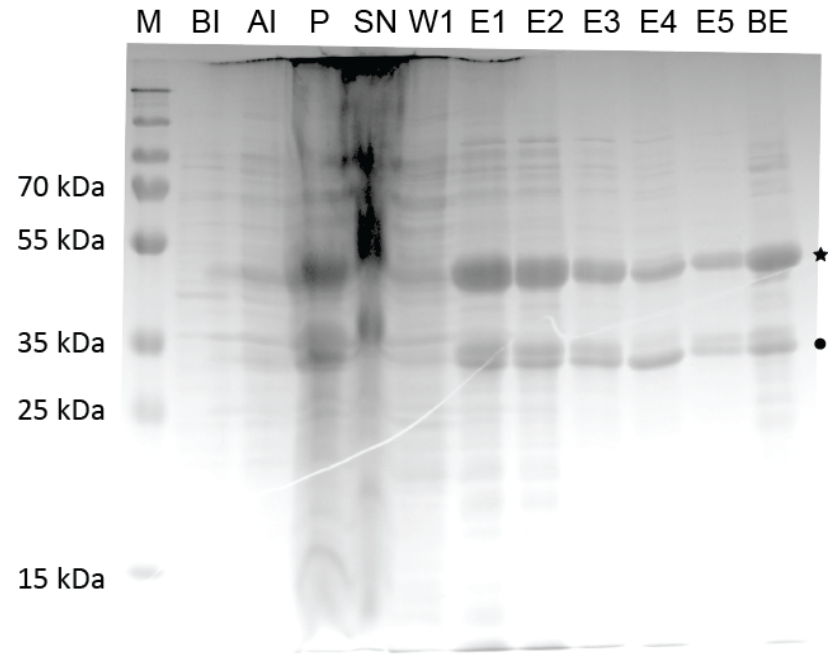

Supplementary Figure 12: Purification of LactC2-eGFP and LactC2-mCherry. Images of SDS-PAGE gels to visualize the purification steps of LactC2-eGFP (**a**) and LactC2-mCherry (**b**). **a**, Recombinant LactC2-eGFP was expressed in *E. coli* and purified using Ni-NTA chromatography column. "1" stands for the protein produced by strain Rosetta ER2566, "2" by strain Rosetta 2; "PI" stands for post-induction with IPTG, "S" for the supernatant and "P" for the pellet, both after cell lysis by sonication, "FT" for the flow-through of the membrane binding step, "W" for the flow-through of the column washing step, "E" for eluate and "BE" for the final purified protein after buffer exchange. The white boxes indicate the expected region for the protein band. Double bands occurring in lane E1 can hint at incomplete

reduction or denaturation of the protein. **b**, In lane “M” 5 µL of Page ruler plus ladder (Promega) were loaded. In the following lanes a sample of the expression strain before induction (BI), after overnight induction at RT (AI), the pellet after lysis and centrifugation (P), the supernatant after lysis (SN), the first washing step (W1), elutions 1 to 5 (E1-E5) and a sample after buffer exchange (BE). The expected product size of the fusion protein is 47 kDa corresponding to the bands marked by a star. The dot marker indicates a set of two bands roughly corresponding to a monomeric mCherry protein including the T7 tag (30 kDa). Two batches of LactC2-eGFP and LactC2-mCherry were prepared on different days and similar purification results were obtained on gel.

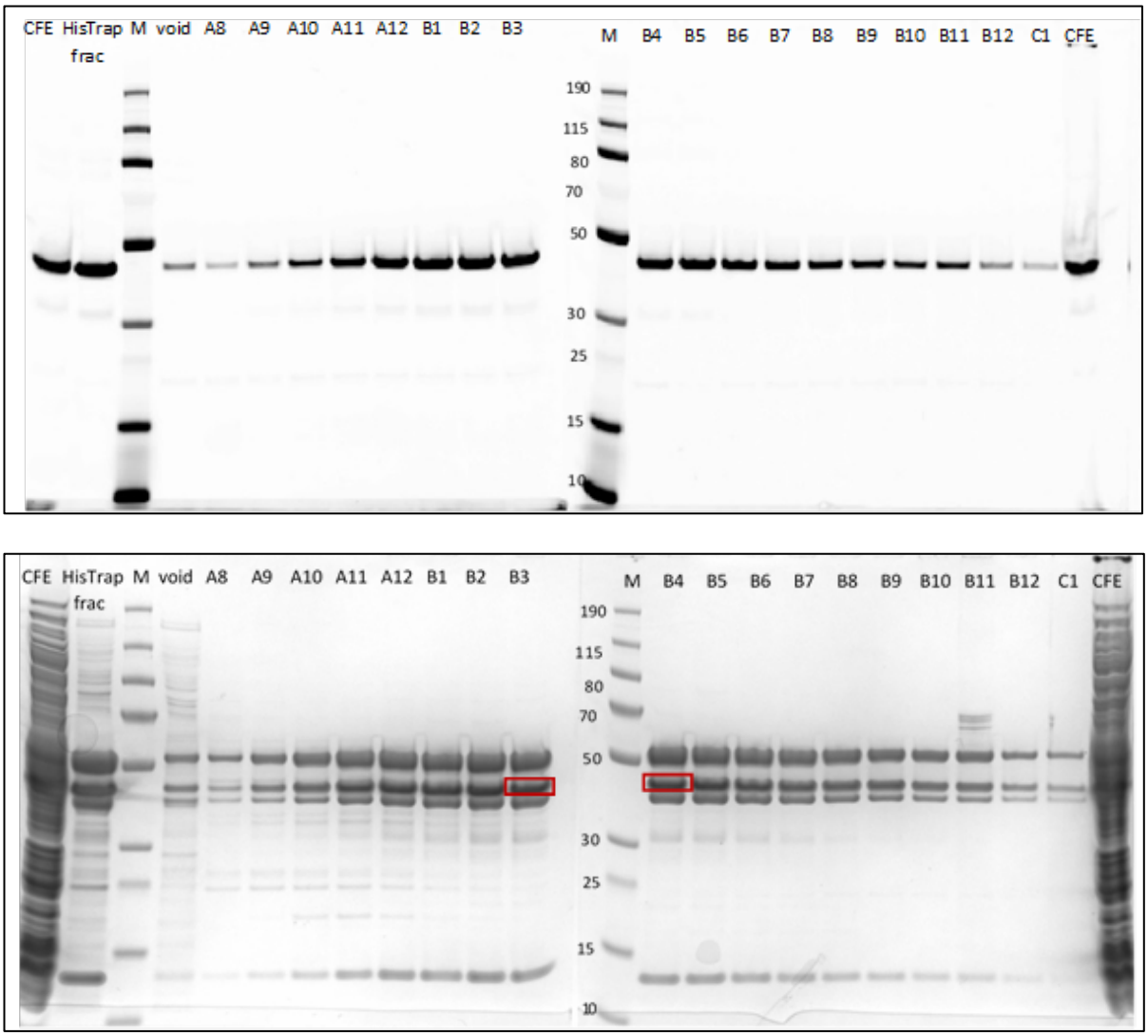

Supplementary Figure 13: Analysis of gel filtration fractions of purified LactC2-mCherry on 4-12% Bis-Tris SDS-PAGE gels. Samples from different purification steps were loaded on the gels. The upper panel shows a fluorescence image of the gels to localise the folded, active mCherry. The bottom panel shows the same gels stained with Coomassie to visualise the total protein content. The red boxes indicate the fluorescent band of the native mCherry fusion protein. The other two prominent bands above and below very likely correspond to differently denatured states of the mCherry, similar to what Mestrom et al. observed [3]. CFE, cell-free extract; HisTrap frac, pooled HisTrap fractions corresponding to the starting material for gel filtration; M, PageRuler^{TM} Plus Prestained protein ladder (ThermoFisher); void, void volume of column; A8 to C1, gel filtration fractions. The molecular weight markers on lane 'M' are in kDa. These experiments were performed twice and similar results were obtained.

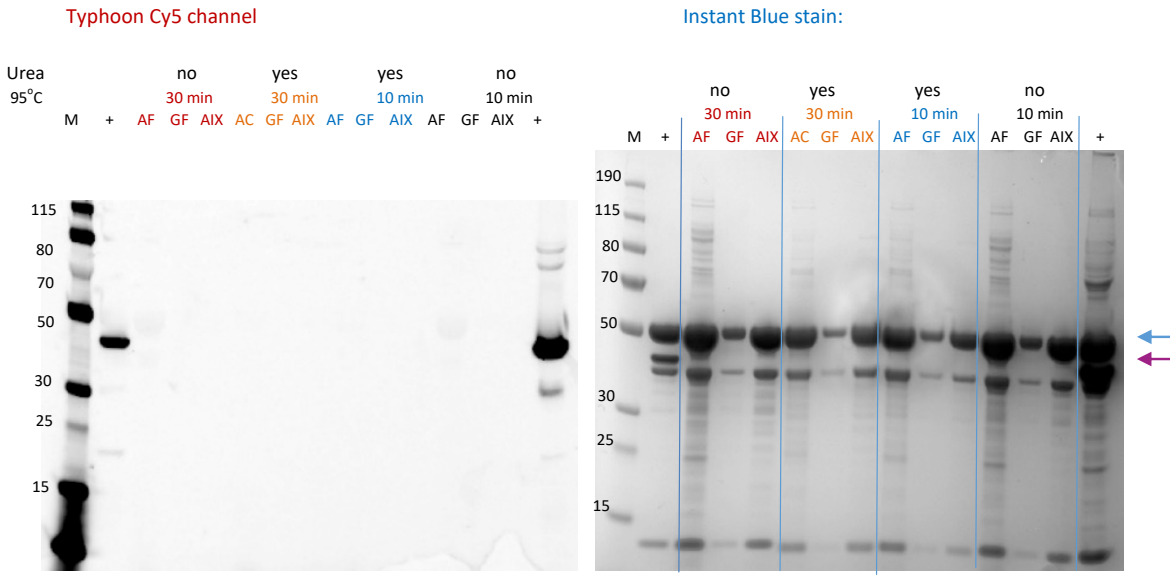

Supplementary Figure 14: SDS-PAGE analysis of LactC2-mcherry samples subjected to different denaturing conditions. The left panel shows a fluorescence image, where only the folded, active mCherry can be seen. The right panel shows the same gel stained with Coomassie to visualise the total protein content. AF, affinity chromatography; GL, gel filtration chromatography; AIX, anion exchange chromatography. The time in minutes indicates the duration of the treatment at 95 °C in Laemmli sample buffer supplemented with 10 mM DTT. The 'yes' or 'no' refers to the addition, or not, of 2 M urea in the sample loading buffer. The blue arrow points to the fully denatured LactC2-mCherry. The magenta arrow indicates the native protein, of which the mCherry fluorescence disappears after heat treatment. The 'M' lane is the ladder in kDa. The lane '+' corresponds to gel filtration sample in Bolt 4xLDS sample buffer (ThermoFisher) incubated for 10 minutes at 75 °C. These experiments were performed twice and similar results were obtained.

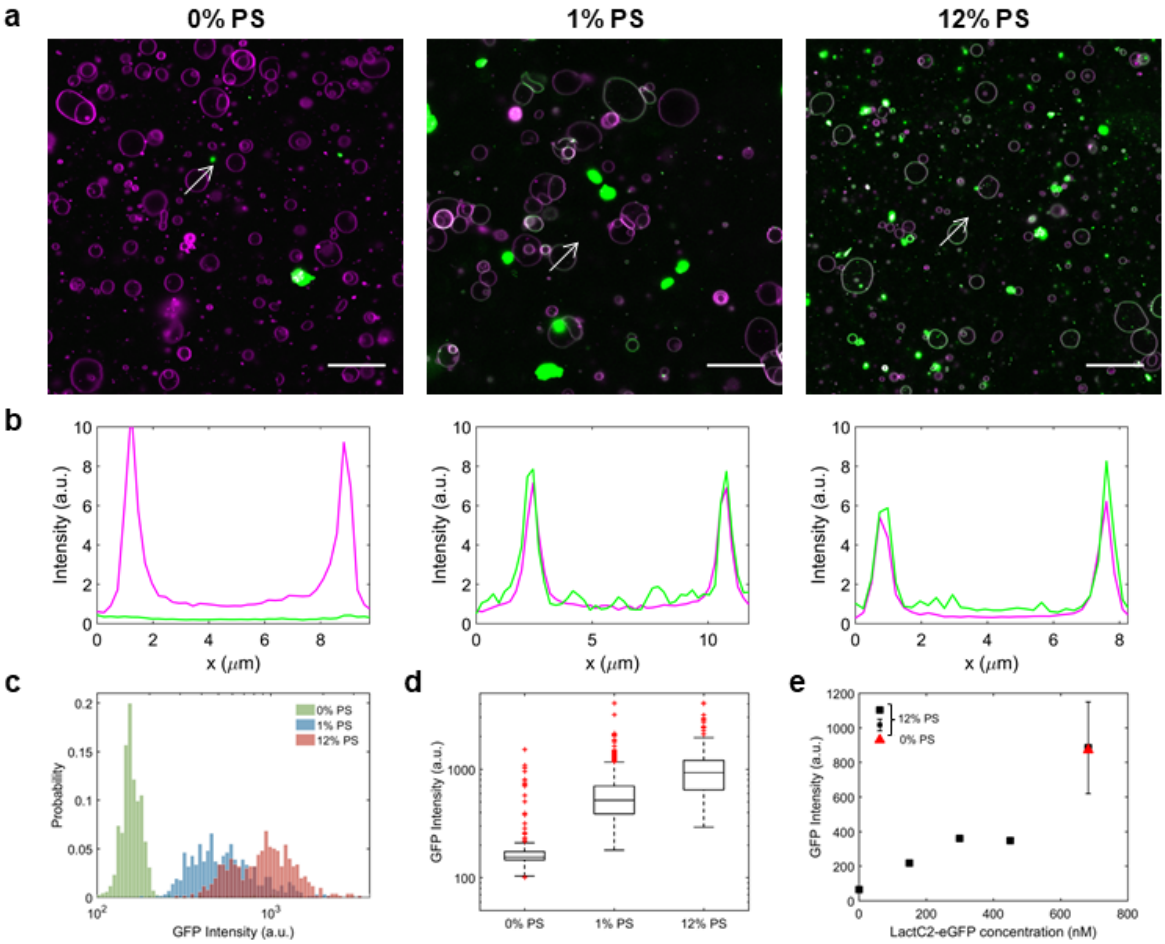

Supplementary Figure 15: LactC2-eGFP specifically binds to PS-containing liposomes. a Confocal fluorescence images of liposomes (membrane in magenta) containing 0%, 1%, or 12% DOPS in the membrane. The liposomes were incubated with 150 nM of LactC2-eGFP (green signal) before imaging. Green spots are LactC2-eGFP aggregates, which were typically observed in all conditions and do not colocalize with vesicles. All experimental conditions have been tested twice and similar results were obtained. Scale bars represent 20 µm. **b**, Fluorescence intensity line profiles corresponding to the arrows appended in **a**. Texas Red membrane dye signal is in magenta and LactC2-eGFP signal is in green. Clear signal colocalization can be seen in the presence of 1% and 12% PS. **c**, Average LactC2-eGFP rim intensity for 0%, 1% and 12% PS. The distributions of LactC2-eGFP fluorescence at 1% and 12% PS significantly overlap. Number of analysed liposomes N = 675, 560, 496, respectively. **d,** Box plot of the data displayed in **c**. N = 675, 560, 496 (from left to right). The box represents all data point between the 25th and 75th percentile, with the line indicating the median. Whiskers extend the most extreme data points not considered outliers. Outliers are plotted individually as red '+' signs. The relationship between LactC2-eGFP fluorescence intensity and PS concentration is nonlinear. **e**, Average LactC2-eGFP rim intensity for liposomes with 0% or 12% PS and varying concentrations of LactC2-eGFP.

For 12% PS, *N* = 503, 273, 93 and 403 liposomes (from left to right), all from one experiment. The error bar corresponds to the mean ± SD of two 12% PS samples, with *N* = 314 and *N* = 71. The red triangle represents the average GFP intensity of 60 liposomes, from one experiment, for liposomes containing 0% PS. Clear non-specific binding of the LactC2-eGFP probe to the membrane can be observed at high concentration. To ensure PS-binding specificity, a working concentration of LactC2-eGFP of 150 nM was employed in all measurements with expressed pGEMM7. a.u., arbitrary unit. Source Data are available for panels **c-e**.

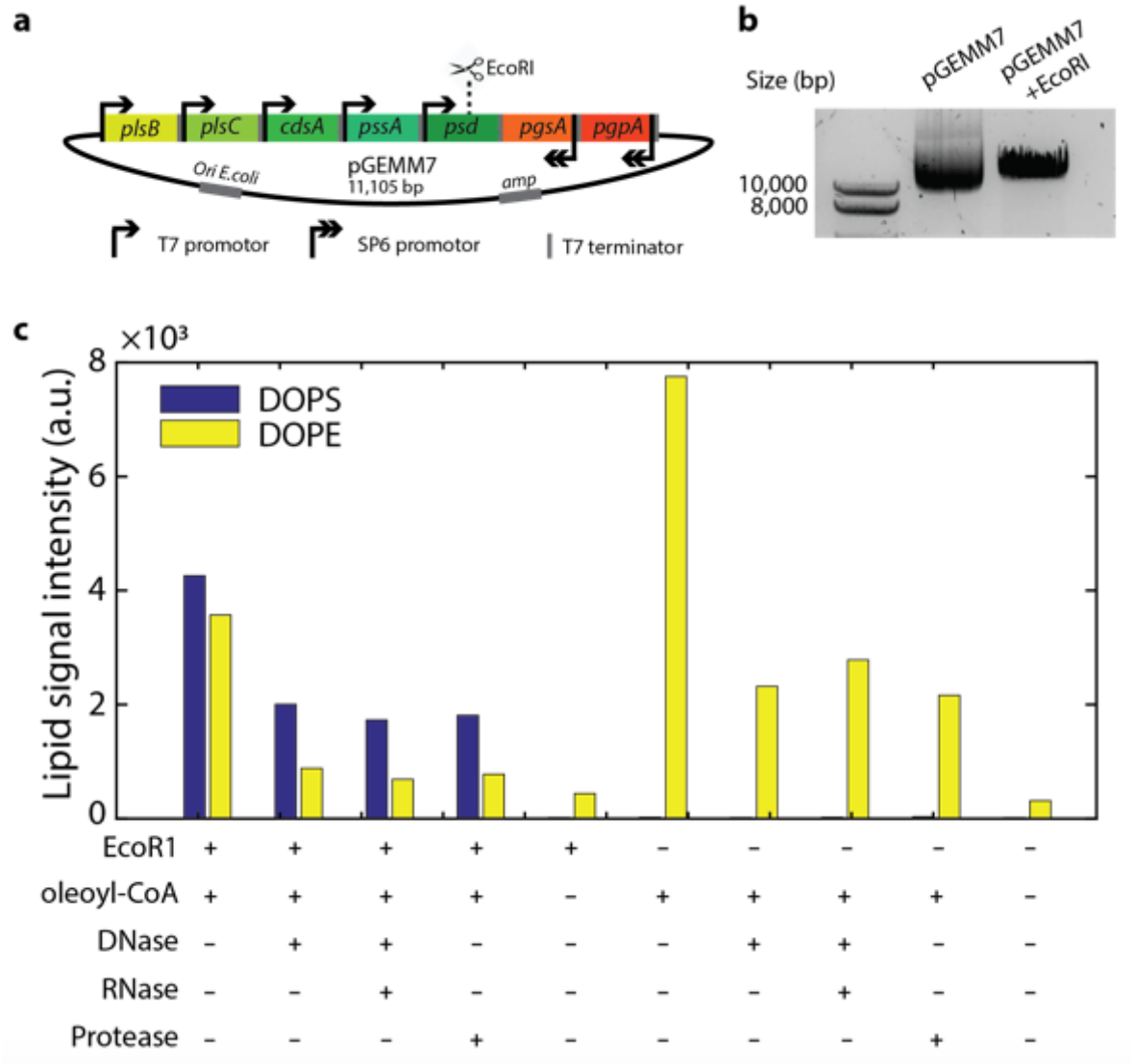

Supplementary Figure 16: Expression of EcoRI-restricted pGEMM7 results in accumulation of phosphatidylserine. a, Schematic representation of the pGEMM7 plasmid map. The EcoRI site in the *psd* gene is depicted. **b**, 1% agarose gel showing unrestricted pGEMM7 and pGEMM7 cleaved with EcoRI. Similar digestion patterns have been observed across >3 repeats. **c**, LC-MS analysis of synthesized DOPS and DOPE with circular pGEMM7 (–EcoRI) or linearized pGEMM7 (+EcoRI) expressed inside giant liposomes. No SP6 RNAP was added. The total integrated counts for DOPS and DOPE are shown. Accumulation of PS is only observed with the linear DNA template, i.e. when expression of the Psd enzyme which converts PS into PE is inhibited. Some residual PE synthesis is observed, probably due to incomplete enzymatic digestion of pGEMM7. Various methods to confine gene expression to the inside of vesicles have been tested. Using proteinase K or DNase gave equivalent results, corroborating the findings presented in the main text **Fig. 3a**. Source Data are available for panel **c**.

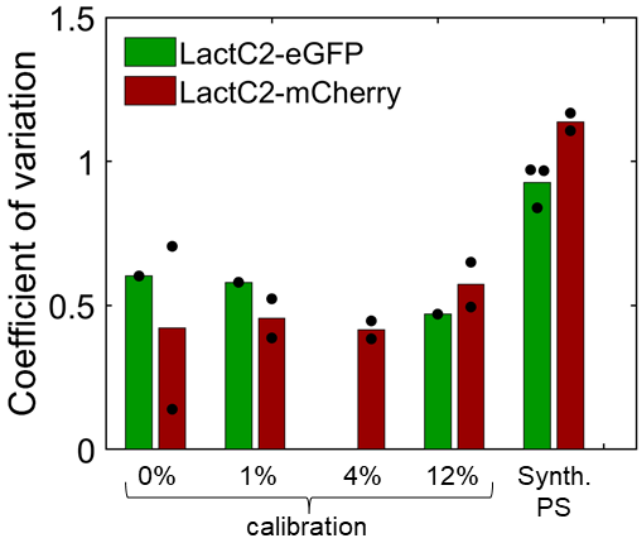

Supplementary Figure 17: Liposome-compartmentalized PS synthesis results in a higher coefficient of variation in LactC2-eGFP signal than when PS is directly included in the vesicle membrane. The coefficient of variation was defined as σ/μ, where σ the standard deviation and μ the mean, of the LactC2-eGFP or -mCherry signal. It provides a good measure of the excess liposome-to-liposome heterogeneity of membrane-incorporated PS caused by cell-free protein and lipid synthesis. The coefficient of variation was calculated for control samples with liposomes containing a fixed amount of PS (0, 1, 4 or 12 mol. %, as indicated) and for in-liposome synthesized PS samples. Liposome-confined synthesis of PS results in higher values of the coefficient of variation with both fluorescent probes, providing a quantitative measure of the liposome-to-liposome heterogeneity in the yield of synthesized PS. Black dots indicate coefficients of variation derived from independent experiments, and bar height represents the mean coefficient of variation of these experiments. The number of independent repeats is indicated by the number of data points shown. Source Data are available.

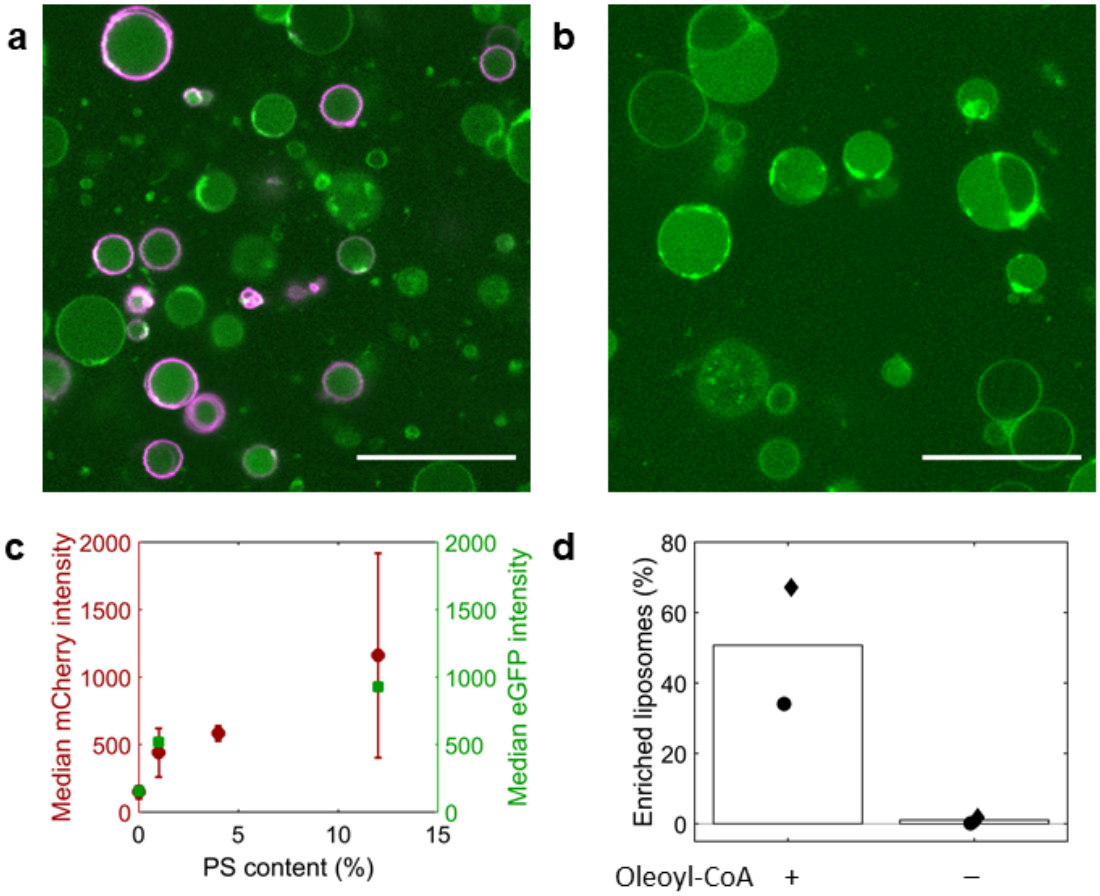

Supplementary Figure 18: LactC2-mCherry is also a compatible PS-specific binding probe. Confocal fluorescence images of liposomes encapsulating all necessary components for pGEMM7Δ*psd*-directed lipid synthesis, in the presence (**a**) or absence (**b**) of oleoyl-CoA. Both conditions were tested twice and similar results were obtained. LactC2-mCherry signal is displayed in magenta. Since mCherry is not spectrally compatible with the Texas Red membrane dye, liposomes were alternatively stained by addition of acridine orange (AO, green). AO is commonly used as a nucleid acid dye, but we have previously observed that the hydrophobic molecule partitions also into liposome membranes [7]. Compared with the eGFP fusion protein, less prominent clusters of LactC2-mCherry were observed. Scale bar represents 20 µm. **c**, Median LactC2-mCherry intensity values for liposomes containing various amounts of PS (indicated in mol. %). Data are the mean ± SD from three repeats. Data obtained with LactC2-eGFP (**Supplementary Fig. 15**) are superimposed for comparison. **d**, Percentage of PS-enriched liposomes after expression of pGEMM7Δ*psd* in the presence or absence of oleoyl-CoA. Bars represent the mean from two independent repeats. Individual data points are marked with a different symbol. Results are similar as with LactC2-eGFP (main text **Fig. 5e**), demonstrating that the nature of the fluorescent protein does not influence the membrane binding ability, despite the fact that LactC2-eGFP is more prone to aggregation. Source Data are available for panels **c** and **d**.

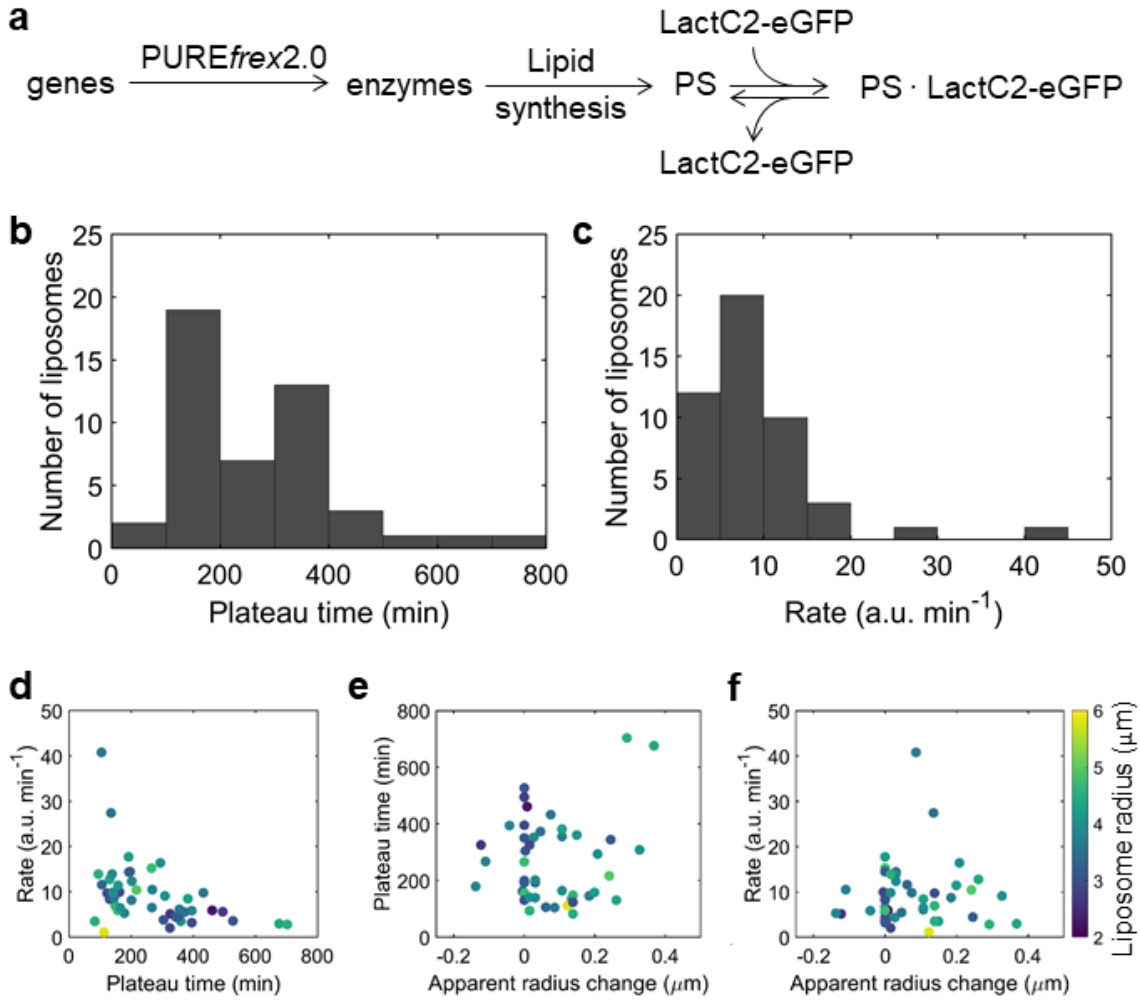

Supplementary Figure 19: Kinetic analysis of combined enzyme expression, PS synthesis, and LactC2-eGFP binding. a, Overview of the main kinetic steps resulting in binding of LactC2-eGFP to synthesized PS, as observed in main text **Figs. 5,6**. **b**, **c**, Histograms, for the 47 traces shown in **Fig. 6b**, of plateau time (**b**) and apparent rate (**c**), as defined in Eq. 2 and Eq. 3, respectively. **d**, Scatter plot of the plateau time and apparent rate as shown in **b** and **c**. Color coding corresponds to the (apparent) liposome radius [4]. No clear size dependence can be observed. Plateau time and rate are somewhat negatively correlated (Pearson's correlation coefficient $\rho = -0.44$). **e**, **f**, The plateau time (**e**) and rate (**f**) have been plotted against the apparent radius change. Color coding and the analysed liposomes are the same as in **d**. Source Data are available for panels **b**-**f**.

SUPPLEMENTARY REFERENCES

[1] Van Nies, P., Canton, A. S., Nourian, Z. & Danelon, C. Monitoring mRNA and protein levels in bulk and in model vesicle-based artificial cells. *Methods Enzymol* **550,** 187-214 (2015).

[2] He, B., Rong, M., Lyakhov, D., Gartenstein, H., Diaz, G., Castagna, R., et al. Rapid mutagenesis and purification of phage RNA polymerases. *Protein Expression and Purification* **9,** 142-151 (1997).

[3] Mestrom, L., Marsden, S.R., Dieters, M., Achterberg, P., Stolk, L., Bento, I., Hanefeld, U., Hagedoorn, P.L. Artificial fusion of mCherry enhances trehalose transferase solubility and stability. *Appl. Environ. Microbiol.* **85,** e03084-18 (2019).

[4] Blanken, D., Van Nies, P., & Danelon, C. Quantitative imaging of gene-expressing liposomes reveals rare favorable phenotypes. *Phys. Biol.* **16,** 045002 (2019).

[5] Godino, E., et al. De novo synthesized Min proteins drive oscillatory liposome deformation and regulate FtsA-FtsZ cytoskeletal patterns. *Nat. Commun.* **10,** 4969 (2019).

[6] Scott, A., et al. Cell-free phospholipid biosynthesis by gene-encoded enzymes reconstituted in liposomes. *PLoS One* **11,** e0163058 (2016).

[7] Van Nies, P., et al. Self-replication of DNA by its encoded proteins in liposome-based synthetic cells. *Nat. Commun.* **9,** 1583 (2018).